

Static impedance functions for monopiles supporting offshore wind turbines in nonhomogeneous soils-emphasis on soil/monopile interface characteristics

Younes Abed¹, Djillali Amar Bouzid^{*1}, Subhamoy Bhattacharya²
and Mohammed H. Aissa³

¹Department of Civil Engineering, Faculty of Technology, University Saad Dahled of Blida, Route de Soumaa, Blida 09000, Algeria

²Department of Civil and Environmental Engineering, Tomas Telford Building, University of Surrey, Surrey GU2 7HX, UK

³Department of Material Engineering, Faculty of Sciences and Technology, University of Médéa, Quartier Ain D'hab, Médéa 26000, Algeria

(Received July 29, 2015, Revised March 8, 2016, Accepted April 1, 2016)

Abstract. Offshore wind turbines are considered as a fundamental part to develop substantial, alternative energy sources. In this highly flexible structures, monopiles are usually used as support foundations. Since the monopiles are large diameter (3.5 to 7 m) deep foundations, they result in extremely stiff short monopiles where the slenderness (length to diameter) may range between 5 and 10. Consequently, their elastic deformation patterns under lateral loading differ from those of small diameter monopiles usually employed for supporting structures in offshore oil and gas industry. For this reason, design recommendations (API and DNV) are not appropriate for designing foundations for offshore wind turbine structures as they have been established on the basis of full-scale load tests on long, slender and flexible piles. Furthermore, as these facilities are very sensitive to rotations and dynamic changes in the soil-pile system, the accurate prediction of monopile head displacement and rotation constitutes a design criterion of paramount importance.

In this paper, the Fourier Series Aided Finite Element Method (FSAFEM) is employed for the determination of static impedance functions of monopiles for OWT subjected to horizontal force and/or to an overturning moment, where a non-homogeneous soil profile has been considered. On the basis of an extensive parametric study, and in order to address the problem of head stiffness of short monopiles, approximate analytical formulae are obtained for lateral stiffness K_L , rotational stiffness K_R and cross coupling stiffness K_{LR} for both rough and smooth interfaces. These expressions which depend only on the values of the monopile slenderness L/D_p rather than the relative soil/monopile rigidity E_p/E_s usually found in the offshore platforms designing codes (DNV code for example) have been incorporated in the expressions of the OWT natural frequency of four wind farm sites. Excellent agreement has been found between the computed and the measured natural frequencies.

Keywords: semi-analytical FE analysis; laterally loaded short monopiles; monopile head stiffnesses; offshore wind turbines; natural frequency

*Corresponding author, Professor, E-mail: d_amarbouzid@yahoo.fr

1. Introduction

1.1 Energy for people seeking cost effectivity and clean energy

In order to meet the world's constantly rising energy demands, the society concern is growing about the use of fossil fuels. Due to the tremendous rising of prices of this source of energy, it is certainly desirable if not mandatory to search for alternatives that are safe, cost effective and may reduce the CO₂ gas emission in the aim to preserve the environment. Offshore wind farms (OWF) are expected to fulfill these requirements and become significant providers of electricity production in modern societies and worldwide. Although wind energy certainly has the potential to play an important role in a sustainable future world energy supply, a number of challenges are still to be met in wind turbine technology. One of those challenges concerns the correct determination of the dynamic characteristics caused by structural vibrations of the individual turbine components (such as rotor blades, gearbox and tower) (Bhattacharya 2014)

1.2 Foundation options for offshore wind turbines

One of the major difficulties encountered in relation to offshore wind turbine (OWT) foundations is the connection of the structure to the seabed and in particular how the foundations should safely transfer the applied loads to the surrounding soil. Furthermore, as the wind turbines are installed in a harsh environment, they must be more reliable than onshore turbines due to higher service and repair costs at such sites. Several different solutions have been developed for different water depths (Luqing *et al.* 2014), all of which meet these criteria. The main concepts are illustrated in Fig. 1.

In shallow waters (0-30 m) a simple concrete 'gravity base' foundations (Fig. 1(b)) are usually used to support OWT. These foundations withstand applied loads and overturning moments by means of their own self weight. The performance of this kind of foundations may be improved by adding ballast after installation. A monopile (Fig. 1(a)) consists of large diameter open-ended steel tube driven into the soil. It is installed by either drilling or grouting and it must be able to transfer both lateral and axial forces to seabed soil. The monopiles are considered to be the best solution for intermediate depths, due to the ease and speed of installation and cost of construction. However, this solution becomes impossible when the water becomes deeper (50-200 m) and the offshore wind turbine larger. This, is due to the impossibility to handle a monopile with the current technology. In this situation, a multiple footing option would be more appropriate, either in the form of a tripod (three foundations) (Fig. 1(c)) or tetrapod (four foundations).

Jacket structures (Fig. 1(d)) consist of three or four legged steel lattice frame supported by single piles placed below each leg. This kind of foundations, which proved its success in deep waters (depths ranging from 35 to 60 m), is employed to transfer the applied loads through the jacket structure to the piles. Finally, founding structures directly to the seabed at depths ranging between 50 m and 200 m, is both impractical and highly expensive, which is why several floating solutions (Fig. 1(e)) have been suggested that rely on buoyancy of the structure to resist overturning. One shortcoming in these is the floating motion which raises additional dynamic loads to the structure. Thus, in despite of the larger wind potential at such depths far from shore, these solutions are still under development.

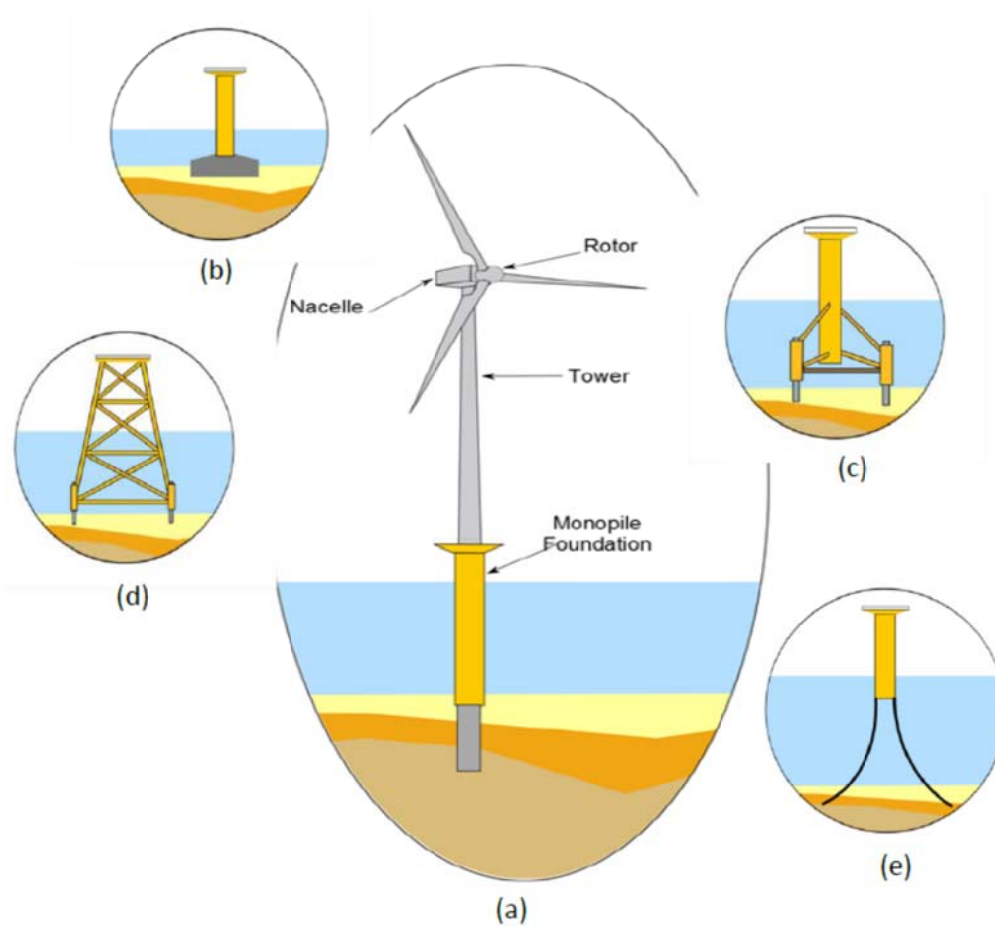


Fig. 1 Offshore wind turbine foundation options: (a) Monopile, (b) Gravity base, (c) Tripod, (d) Jacket and (e) Floating structure

1.3 Monopiles as a most common foundation type and shortcomings in their design existing standards

Up to now, the commonest form of foundation at intermediate depth (up to 35 m) is the monopile foundations, as they have proven to be an efficient solution (Bhattacharya *et al.* 2012, Shirzadeh *et al.* 2013, Lombardi *et al.* 2013, Ki-Yong *et al.* 2013, Lu-Qing *et al.* 2015, Bisoi and Haldar 2015).

When dealing with horizontally loaded single monopiles, generally the lateral monopile response is distinguished into two main categories, namely flexible monopile behavior and rigid monopile behavior. In rigid monopiles a ‘toe kick’ occurs, while in slender monopiles only the upper part of the monopiles participates in the movement. Consequently, the main distinguishing key between the two behaviors is what is called the critical length or critical slenderness L_c/D_p (where L_c is the critical length and D_p is the monopile diameter).

The shortcomings in the existing standards for designing OWT foundations come from the fact

that the designers are confusing between the behavior of short monopiles and slender ones. Although this fact has been clearly addressed by many researchers, decades ago, the current API/DNV design standards are still depending on methods proposed by Reese *et al.* (1974) and which have been originally developed on testing slender piles. This empiricism underpins the major limitations of API RP2A (API, 2011).

Standards for designing laterally loaded piles, e.g., the American Petroleum Institute (API 2011), Det Norske Veritas (DNV 2004) or Germanischer Lloyd (GL 2005) are based on the P-Y curves method. The P-Y curves method, which describes the nonlinear relationship between pile deflection Y and soil reaction P , is based on the work performed in the early 1970s (Reese *et al.*, 1974; Matlock, 1970 and Murchisson and O'Neill, 1984). Although, they have been employed for designing offshore piled foundations by the offshore oil and gas industry for decades, design recommendations (API, and DNV) are not appropriate for designing foundations for offshore wind turbine structures, for many reasons:

a) They have been developed on the basis on full-scale load tests on long, slender and flexible piles with a diameter of 0.61 m, whereas monopiles are relatively shorter and stiffer piles with diameters up to 6.0 m in the offshore wind turbine industry.

b) The widely used API model is calibrated against response to a small number of cycles for offshore fixed platform applications. However, an offshore wind turbine may undergo 10^7 - 10^8 cycles of loading over its lifetime of 20-25 years.

c) Under cyclic loading, the API and DNV models always predict degradation of foundation stiffness in sandy soil. However, many researchers (Adhikari and Bhattacharya 2011, Adhikari and Bhattacharya 2012, Leblanc 2009, Cuéllar *et al.* 2012, Achmus *et al.* 2009) showed that the monopile stiffness in sandy soil will increase as a result of densification of soil in the vicinity of the monopile.

The behavior of monopiles foundations for offshore wind turbines deviate from classical assumption and accumulated experience mainly due to their large diameter, reduced slenderness and high ratio of lateral to vertical loads. The harsh offshore environment poses another challenge of large numbers of load cycles from wind and waves. This behavior is still not well understood and also not being introduced in current design guidelines.

1.4 Purpose and scope of the paper

As far as the accurate prediction of the monopile head displacement and rotation, is concerned, the analysis using the Finite Element Method (FEM) is an excellent tool to narrow the gap between predicted and measured results. Indeed, the use of the Fourier Series Aided Finite Element Method has proven to be an excellent approach to analyze the behavior of laterally loaded monopiles embedded in elastic media.

In this paper, this approach is employed for the determination of static impedance functions of monopiles for OWT subjected to horizontal force and/or to an overturning moment, where a non-homogeneous soil profile has been considered. On the basis of an extensive parametric study, and in order to address the problem of head stiffness of short monopiles, approximate analytical formulae are obtained for lateral stiffness K_L , rotational stiffness K_R and cross coupling stiffness K_{LR} for both rough and smooth pile/soil interfaces. These expressions which depend only on the value of the monopile slenderness L/D_p rather than the relative soil/monopile rigidity E_p/E_s usually encountered in the offshore platforms designing codes (DNV code for example) have been incorporated in the well established expressions of the OWT natural frequency of four wind farm

sites chosen from the literature. These include: walney1 wind farm site (UK), North Hoyle (the Netherlands), Irene Vorrink (the Netherlands) and Lely A2 (UK).

2 .Fourier Series Aided Finite Element (FSAFE) approach used in this study

The problem of an embedded monopile (Fig. 2) under lateral and moment loading is a problem of axisymmetric solids subjected to non-axisymmetric loads. It is a three-dimensional problem, in the sense that all three displacement components are in general nonzero. Similarly, all six stress components are in general nonzero. This type of problems can be analyzed by a semi-analytical approach which as proposed by (Wilson 1965, Winnicki and Zienkiewicz 1979). It consists of expressing forces and displacements in the direction of revolution in a form of Fourier series, calculating the response to each Fourier term and superposing results (Griffiths and Lane 1990, Potts and Zdravkovic 1999). An essential requirement of this approach is that the material properties in the circumferential direction remain constant.

As this approach has already been described in many finite element textbooks (Potts and Zdravkovic 1999, Cook *et al.* 2002), we will only give a brief description.

2.1 Expansion of loading and displacements in Fourier series

In the present problem, it is convenient to adopt a cylindrical coordinate system for the semi-analytical FE formulation. The nodal loads applied to the axisymmetric structure can be expanded in Fourier series as

$$\begin{pmatrix} R(r, z, \theta) \\ Z(r, z, \theta) \\ T(r, z, \theta) \end{pmatrix} = \begin{pmatrix} \bar{R}_0 + \sum_{i=1}^{\infty} (\bar{R}_i(r, z) \cos i\theta + \bar{\bar{R}}_i(r, z) \sin i\theta) \\ \bar{Z}_0 + \sum_{i=1}^{\infty} (\bar{Z}_i(r, z) \cos i\theta + \bar{\bar{Z}}_i(r, z) \sin i\theta) \\ \bar{T}_0 + \sum_{i=1}^{\infty} (\bar{T}_i(r, z) \sin i\theta - \bar{\bar{T}}_i(r, z) \cos i\theta) \end{pmatrix} \quad (1)$$

Where symbols, R , Z and T indicate respectively the radial, axial and the circumferential (hoop) components. All barred quantities are amplitudes, which are functions of r and z but not of θ . Single barred amplitudes represent symmetric load components (loads which have $\theta=0$ as plane of symmetry), while double-barred amplitudes represent anti-symmetric load terms.

It is possible to demonstrate (Cook *et al.* 2002) that in a linear analysis, when loads are expanded as in Eq. (1), displacement components are described by Fourier series as well

$$\begin{cases} u_r(r, z, \theta) = \sum_{i=0}^L \bar{u}_{ri} \cos i\theta + \sum_{i=1}^L \bar{\bar{u}}_{ri} \sin i\theta \\ v_z(r, z, \theta) = \sum_{i=0}^L \bar{v}_{zi} \cos i\theta + \sum_{i=1}^L \bar{\bar{v}}_{zi} \sin i\theta \\ w_\theta(r, z, \theta) = \sum_{i=1}^L \bar{w}_{\theta i} \sin i\theta - \sum_{i=0}^L \bar{\bar{w}}_{\theta i} \cos i\theta \end{cases} \quad (2)$$

The index i stands for the harmonic number, and L is the total number of harmonic terms considered in the series. The single barred terms $\bar{u}_{ri}, \bar{v}_{zi}, \bar{w}_{\theta i}$ are amplitudes of displacements that are symmetric with respect to the plane for $\theta=0$. The double barred terms $\bar{\bar{u}}_{ri}, \bar{\bar{v}}_{zi}, \bar{\bar{w}}_{\theta i}$ are the amplitudes of displacements that are anti-symmetric with respect to the plane for $\theta=0$.

Only the first two terms in the Fourier series are needed in most practical situations. Problems for the first term (i.e., $i=0$) are those related to purely axisymmetric problems and consequently well established in the literature. The second term for $i=1$ is required when the loading pattern

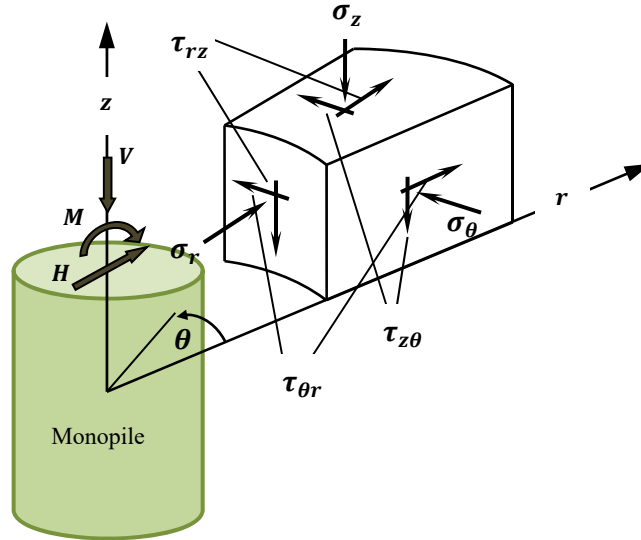


Fig. 2 State of stresses within and around a monopile under vertical and lateral loading

has a plane of symmetry.

For a monopile subjected to a lateral and/or an overturning moment, only the second term for $i=1$ survives, because this loading has a plane of symmetry. In this situation the components of loading in Eq. (1) reduce to

$$R = \bar{R} \cos \theta, Z = \bar{Z} \cos \theta R = \bar{T} \sin \theta \tag{3}$$

Where, \bar{R} , \bar{Z} and \bar{T} are load amplitudes of the first harmonic. The radial \bar{R} amplitude is distributed along the circumference of the monopile. The lateral load H acting as a result of this distribution follows from the expression

$$H = \bar{R} \int_0^{2\pi} \cos^2 \theta \, d\theta = \pi \bar{R} \tag{4}$$

According to the St. Venant's principal the loading of amplitude \bar{R} on the first harmonic will have the same effect as a concentrated force $H = \pi \bar{R}$ acting in the x -direction. Similarly, the vertical \bar{Z} amplitude is distributed along the circumference of the monopile. These tractions generate an overturning moment according to the equation

$$M = D_p \bar{Z} \int_0^\pi \cos^2 \theta \, d\theta = \frac{D_p}{2} \pi \bar{Z} \tag{5}$$

Where D_p is the monopile diameter. Similarly, the tangential \bar{T} amplitude is distributed over the edge of the monopile cross-section. It yields

$$H = -\bar{T} \int_0^{2\pi} \sin^2 \theta \, d\theta = -\pi \bar{T} \tag{6}$$

For the load system as defined by equations 4, 5 and 6, the displacement Eq. (2) reduce to

$$u_r = \bar{u}_r \cos \theta, \quad v_z = \bar{v}_z \cos \theta, \quad w_\theta = \bar{w}_\theta \sin \theta \tag{7}$$

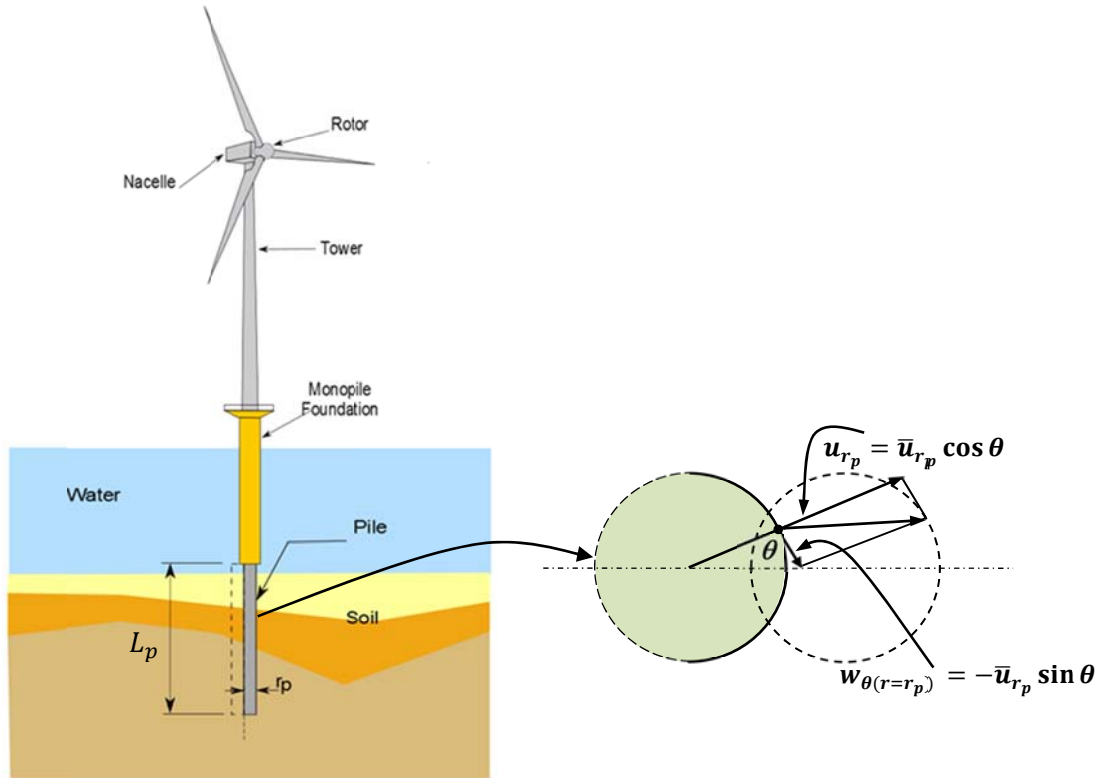


Fig. 3 Displacement components in radial coordinate

Although more work and storage are required than for a genuine 2D analysis, the fact that finite element discretization is only required in radial plane means that band-width problems that occur with 3D elements are avoided. Thus the problem is easier for the analyst when dealing with input and output data.

2.2 Stiffness matrix for volume elements

The stiffness matrix associated with the first harmonic fundamentally depends on the strain-displacement matrix B_v as well as on elasticity matrix D_v . It can be written as

$$K_{vol} = \int_A \int_{-\pi}^{\pi} B_v^T D_v B_v r dr dz d\theta \tag{8}$$

Where A is the cross-section area of the volume finite element. As the matrix B_v is important, it is useful to divide it into sub-matrices. Indeed

$$B_v = [B_1 B_2 \dots \dots B_N] \tag{9}$$

Where B_j is a sub-matrix corresponding to the node j . N is the total number of element nodes. B_j can be written in a more explicit form

$$\mathbf{B}_j = \begin{bmatrix} \frac{\partial N_j}{\partial r} \cos \theta & 0 & 0 \\ 0 & \frac{\partial N_j}{\partial z} \cos \theta & 0 \\ \frac{N_j}{r} \cos \theta & 0 & \frac{N_j}{r} \cos \theta \\ \frac{\partial N_j}{\partial z} \cos \theta & \frac{\partial N_j}{\partial r} \cos \theta & 0 \\ 0 & \frac{N_j}{r} \sin \theta & \frac{\partial N_j}{\partial r} \sin \theta \\ -\frac{N_j}{r} \sin \theta & 0 & \left(\frac{\partial N_j}{\partial r} - \frac{N_j}{r} \right) \sin \theta \end{bmatrix} \tag{10}$$

And the elasticity matrix \mathbf{D}_v is given by

$$\mathbf{D}_v = \frac{E_s}{(1+\nu_s)(1-2\nu_s)} \begin{bmatrix} 1 - \nu_s & \nu_s & \nu_s & 0 & 0 & 0 \\ \nu_s & 1 - \nu_s & \nu_s & 0 & 0 & 0 \\ \nu_s & \nu_s & 1 - \nu_s & 0 & 0 & 0 \\ 0 & 0 & 0 & \frac{1-2\nu_s}{2} & 0 & 0 \\ 0 & 0 & 0 & 0 & \frac{1-2\nu_s}{2} & 0 \\ 0 & 0 & 0 & 0 & 0 & \frac{1-2\nu_s}{2} \end{bmatrix} \tag{11}$$

The integration (in the Eq. (8)) with respect to the circumferential direction can be easily handed if we take profit of the orthogonal properties of the trigonometric functions

$$\int_{-\pi}^{\pi} \sin^2 \theta d\theta = \pi, \quad \int_{-\pi}^{\pi} \cos^2 \theta d\theta = \pi \quad \text{and} \quad \int_{-\pi}^{\pi} \sin \theta \cos \theta d\theta = 0 \tag{12}$$

Then the Eq. (8) will have a more simple form

$$\mathbf{K}_{vol} = \pi \int_A \mathbf{B}_v^T \mathbf{D}_v \mathbf{B}_v r dr dz \tag{13}$$

In what follows, the volume element employed is a ring element having as cross-section, the 2-D eight-noded isoparametric element (Fig. 4). This element which has been used to model both monopile and soil, performs well in analyzing problems involving flexural behavior. Furthermore,

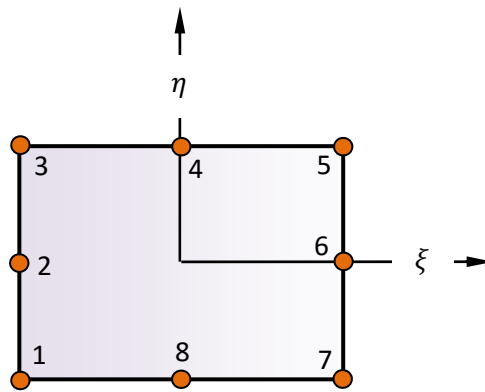


Fig. 4 A ring element with Q8 as cross-section

this element has a quadratic field of displacements, and consequently it constitutes a well compromise between complexity and accuracy (Durocher *et al.* 1978). This element is illustrated in Fig. 4.

The shape functions associated to this element are:

- At corner nodes: 1,3,5 and 7

$$N_j = \frac{1}{4}(1 + \xi\xi_j)(1 + \eta\eta_j)(\xi\xi_j + \eta\eta_j - 1) \tag{14}$$

- At mid-side nodes

$$N_j = \frac{1}{2}(1 - \xi^2)(1 + \eta\eta_j) \quad \text{for } j = 4, 8 \tag{15}$$

$$N_j = \frac{1}{2}(1 - \eta^2)(1 + \xi\xi_j) \quad \text{for } j = 2, 6 \tag{16}$$

2.3 Stiffness matrix for soil/monopile interface elements

In most problems of soil-structure interaction, relatively simple models may be adopted for interfaces as they usually involve compressive contact stresses. For many problems it may be convenient to model interface behavior by merely refining a finite element mesh in the immediate vicinity of the interface. However, as the mesh remains continuous and adjacent elements are assigned with considerably different properties, occasional numerical singularities may occur constituting thus, the main drawback of this simple method.

A joint element was thus formulated by Amar Bouzid *et al.* (2004) to model soil/structure interfaces of axisymmetric solids of revolution subjected to non-axisymmetric loading using a semi-analytical analysis. To this end a six-noded interface element was formulated which can be combined with eight or nine-noded quadrilateral volume elements (Fig. 5). A brief outline of the interface formulation will be given here.

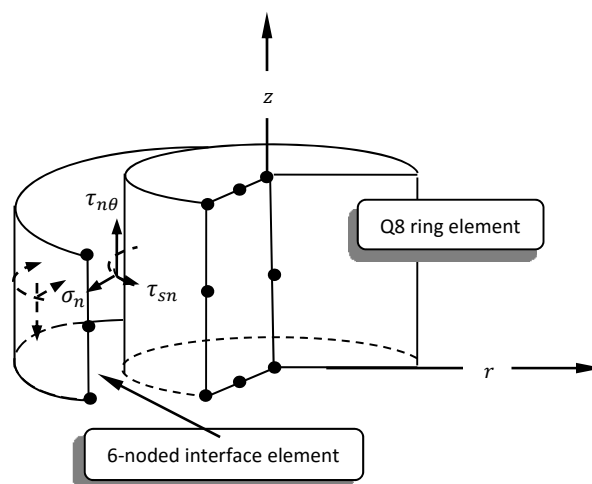


Fig. 5 Zero thickness 6-noded interface element in an axisymmetric body showing the normal and shear stresses acting at the interface location

According to the standard formulation of the displacement-based finite element method (Zienkiewicz and Taylor 2000) the stiffness matrix K_{int} of the interface element is given by the equation

$$K_{int} = \int_A \mathbf{B}_i^T \mathbf{D}_i \mathbf{B}_i dA \tag{17}$$

Where, \mathbf{B}_i is the strain-displacement matrix, \mathbf{D}_i is the interface constitutive matrix and A is the cross-section area of the interface element. The thickness of the interface element is taken to be zero. Since the interface element is a fictive location and is not a material itself, it represents only the interaction between two dissimilar materials. Hence, there will exist only a normal stress, σ_{ni} , and shear stresses, τ_{sni} and $\tau_{n\theta i}$, in this imaginary area. The displacement-stress relationships can be written as

$$\boldsymbol{\sigma}_i = \mathbf{D}_i \mathbf{u}_{rel} \tag{18}$$

Where, $\boldsymbol{\sigma}_i = \begin{Bmatrix} \tau_{sni} \\ \sigma_{ni} \\ \tau_{n\theta i} \end{Bmatrix}$, $\mathbf{D}_i = \begin{bmatrix} k_s & 0 & 0 \\ 0 & k_n & 0 \\ 0 & 0 & k_s \end{bmatrix}$ and $\mathbf{u}_{rel} = \mathbf{B}_i \bar{\mathbf{u}}^e$

The interface shear stiffness k_s and the interface normal stiffness k_n are in units of force per cube length. The vector of radial, axial and circumferential nodal displacement amplitudes in the global coordinate system can be written as $\bar{\mathbf{u}}^e = [\bar{u}_1, \bar{v}_1, \bar{w}_1, \dots, \bar{u}_6, \bar{v}_6, \bar{w}_6]^T$. As in most interface stiffness matrices formulations, the numerical integration has been used, the analytical procedure developed by Amar Bouzid *et al.* (2004) has the advantage to avoid spurious oscillations of stresses over interface area as it is accurately determined.

3. Nonhomogeneous half space selected for this study

A more general, and often appropriate class of soils where deposits of soils have stiffnesses which increase with depth (Cole and Burland 1972, Burland *et al.* 1973, Hooper 1973). This consideration of soil non-homogeneity has proved to be more realistic in many practical cases

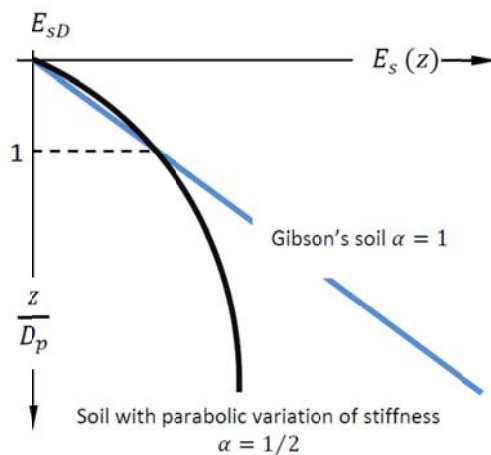


Fig. 6 Variation of soil Young's modulus with depth according to a power law pattern

where the effective stresses increase with depth. The soil modulus is usually taken to have a power law variation with depth (Booker *et al.* 1985) as expressed by the equation

$$E_s(z) = E_{sD} \left(\frac{z}{D_p} \right)^\alpha \tag{19}$$

Where E_{sD} is the soil modulus at a depth z equal to the monopile diameter D_p , and α is an exponent that varies between zero and one. Eq. (19) includes a soil with a parabolic variation of stiffness with depth for $\alpha = 1/2$ and a Gibson's soil for $\alpha = 1$ as shown in Fig. 6.

These idealized profiles are useful as an approximation to various types of soil profiles. The

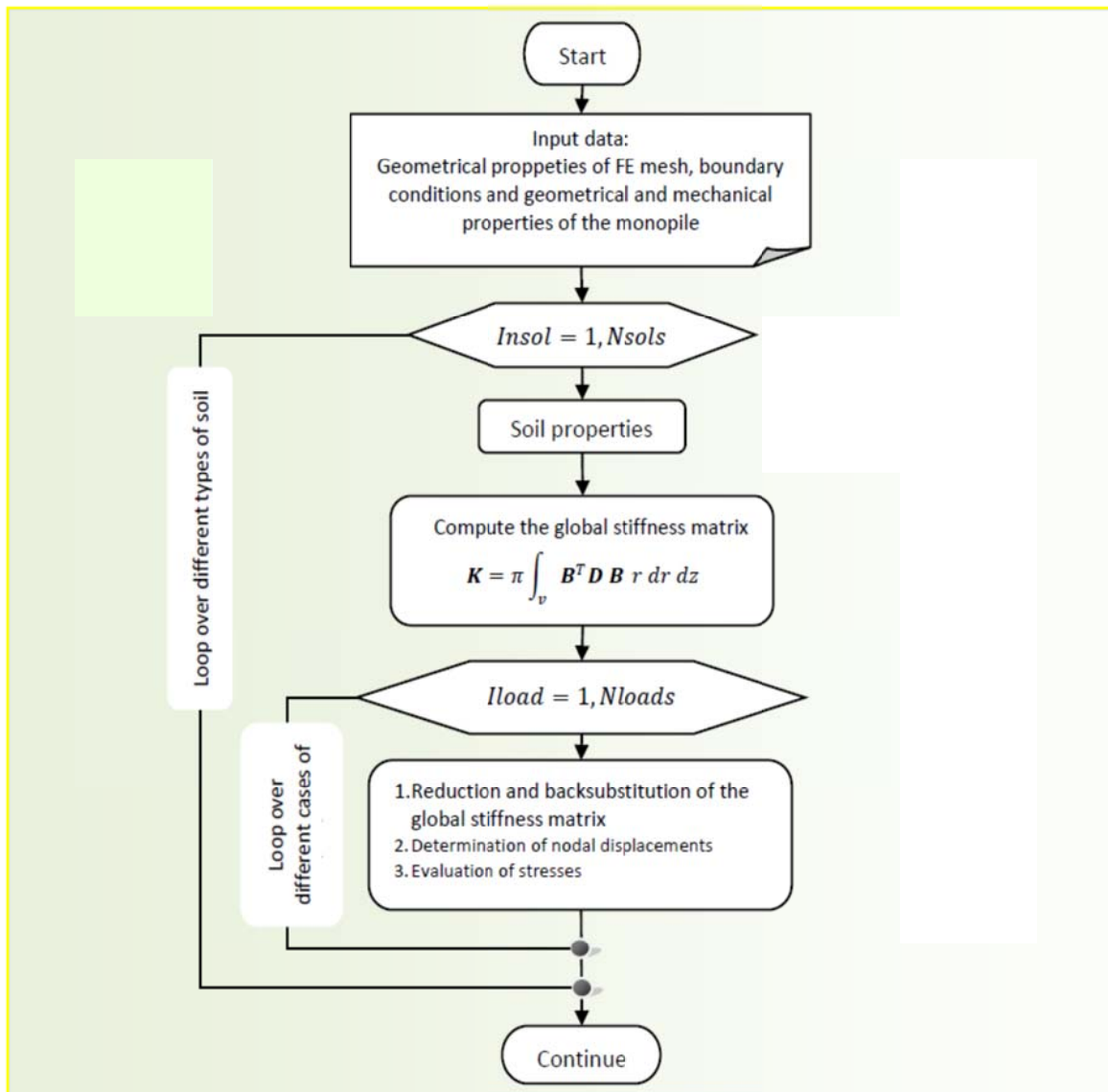


Fig. 7 MPULL_SAA Flowchart

linear distribution with depth models a normally consolidated clay or the degraded shear modulus distribution with depth in a cohesionless soil profile after some cyclic loading. The square root Young's modulus distribution represents cohesionless soils at small strains. For these materials the small strain elastic modulus is known to be a function of square root of the effective stress.

4. Computer Program MPULL_SAA, FE mesh and soil/monopile properties adopted in this study

The theoretical developments of the FSAFEM for the problem of laterally loaded single monopiles presented in subsections (2.1-2.3) have been encoded in a Fortran computer program called **MPULL_SAA**, which stands for **MonoPiles Under Lateral Loading_Semi-Analytical Approach**.

The computer program begins by reading the geometrical characteristics of the FE mesh (number of elements, lateral and bottom distances of the mesh, etc.), interface stiffness properties, boundary conditions, geometrical and mechanical properties of the monopile and soil and certain parameters relevant to the Fourier series harmonic analysis.

Within a loop of all types of soil analyzed, **MPULL_SAA** reads for the soil under consideration, its Young's modulus at a depth equal to one monopile diameter as well as the exponent which controls the variation of soil stiffness with depth. Then, on the basis of the available data, it computes the global stiffness matrix which encompasses the soil, the monopile and the interface separating them.

Within another nested loop which accounts for the loading cases, the global stiffness matrix is soon reduced using Gaussian elimination and a backsubstitution is performed to give the nodal displacements of the whole system.

The **MPULL_SAA** output can show the monopile displacements, monopile rotations, shear forces and bending moments along the monopile shaft at the end of each load case. Fig. 7 shows **MPULL_SAA** flowchart summarizing the different steps of computations.

4.1 Boundary conditions

As far as the simplicity in meshing is concerned, only half of the domain was meshed for the 3D semi-analytical FEM study due to the symmetry of the problem. The mesh used for the study is shown in Fig. 8.

The distances from boundaries are chosen large enough to eliminate the boundary effect. Applied boundary conditions to the soil are pinned support at the bottom with no displacements in the horizontal, vertical and circumferential directions ($u_r = v_z = w_\theta = 0$) and roller support at sides with no movement in the horizontal direction ($u_r = 0$).

The mesh has been refined in areas with stress concentration in the vicinity of the monopile and soil surface. The mesh density decreases at regions close to the boundaries. In finite element modeling a finer mesh typically results in a more accurate solution, while the computation time will increase. By performing a comprehensive FE mesh studies, a sufficiently dense mesh with an accurate solution has been obtained. Four important points can emerge from these studies. Firstly, the mesh need not extend laterally to more than $25 D_p$. Secondly, the mesh need not extend to more than one monopile length under the monopile tip. Thirdly, thirty six (36) eight-noded isoparametric elements are sufficient to model the soil/rigid monopile system in both sides.

Fourthly, ten (10) elements in lateral direction and twenty (20) elements in the vertical direction have been found enough to capture the elastic behavior of the monopile.

4.2 Material properties for soil, interface and monopile

In order to model the smoothness and the roughness of the interface separating the monopile

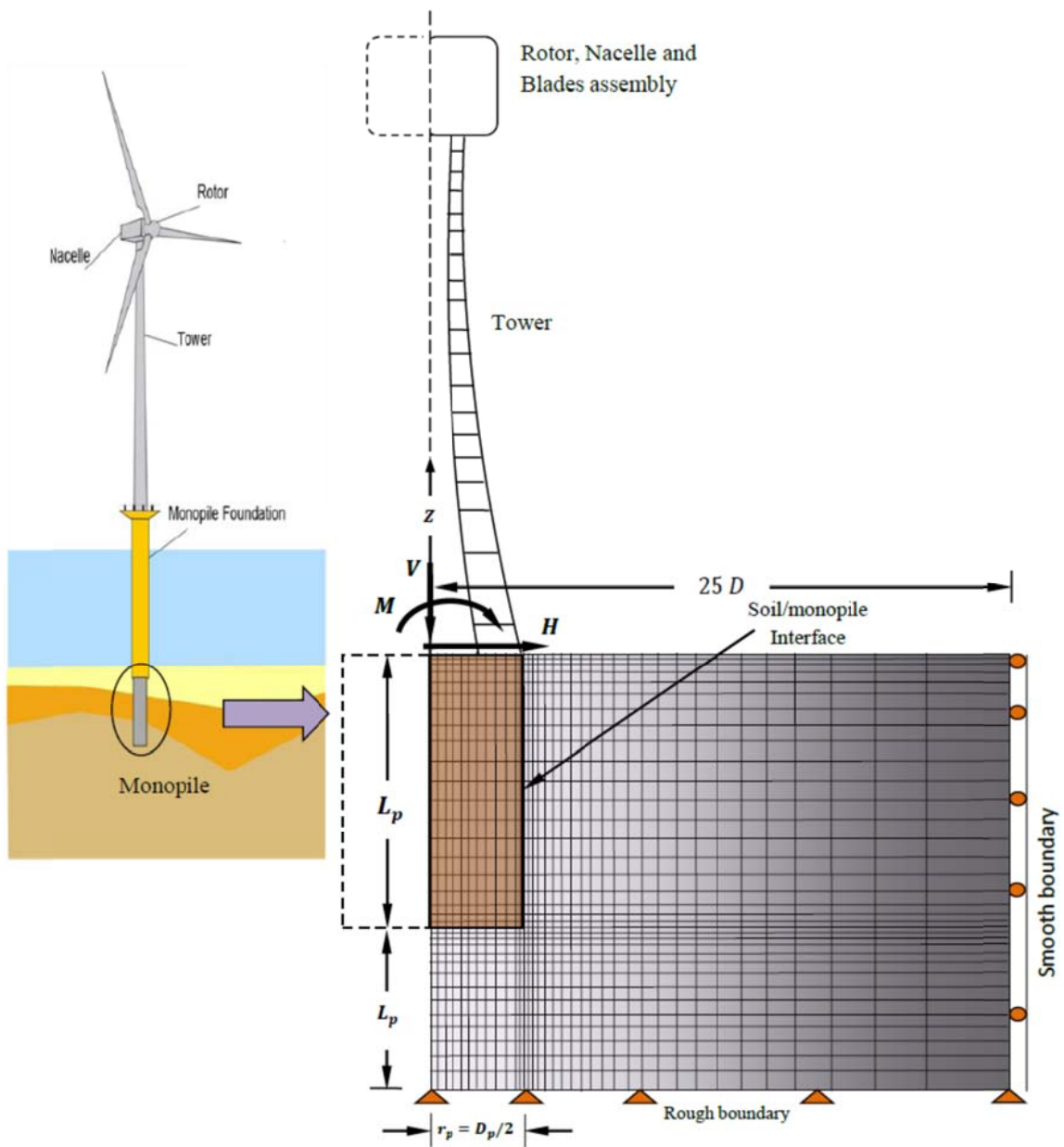


Fig. 8 Finite element mesh of the monopile and the surrounding elastic medium

Table 1 Monopile and interface properties

Monopile properties	Interface properties	
	Smooth interface	Rough interface
$E_p = 2 \times 10^7 \text{ kN/m}^2$	$k_n = 10^{12} \text{ kN/m}^3$	$k_n = 10^{12} \text{ kN/m}^3$
$\nu_p = 0.25$	$k_s = 0.0$	$k_s = 10^{12} \text{ kN/m}^3$

from the surrounding elastic medium, the interface formulation described in the subsection 2.3 has been implemented. Semi-analytical finite element computations have been carried out in an elastic, isotropic soil characterized by a stiffness which varies according to the power law as described in section 3. (Detailed description de the different values of soil Young's modulus and Poisson's ratios considered in the parametric study are given in subsection 5.3).

The rough interface between the rigid monopile and the surrounding medium has been simulated by either prescribing large values for the interface stiffness coefficients or fully removing the interface formulation from the FE code by using a conventional analysis in which soil and monopile are tied together at the shared nodes. For simulating a smooth interface, finite element analyses were carried out by imposing a shear stiffness equal to zero and a large value for the normal stiffness.

The deformation characteristics of the rigid monopile and those of soil/monopile interface are given in Table 1.

5. Finite element establishment of critical length and static impedance functions for monopiles

The overall foundation stiffness is dependent on the strength and stiffness of the soil as well as on the structural foundation elements. The foundation stiffness needs to be determined as a basis for predicting the dynamic structural response to wind, wave and earthquake loading. The foundation stiffness is in general frequency dependent. This is particularly important when predicting dynamic response to earthquake.

The soil that supports a foundation structure usually has finite stiffness. It can therefore usually not be justified to model the soil as a rigid mass. In other words, the foundation structure cannot be assumed to have a fixed support. In any analysis of a foundation structure and of the wind turbine structure that it supports, it is therefore important to model the actual boundary conditions formed by the supporting soils properly.

Static stiffnesses are stiffnesses for frequencies approaching zero. The dynamic stiffnesses may deviate from the static stiffnesses in particular in case of high-frequent vibrations. However, for wind and wave loading of wind turbine foundations, onshore as well as offshore, the induced vibrations will be of such a nature that the static stiffnesses will be representative for the dynamic stiffnesses that are required in structural analyses.

5.1 Critical slenderness ratio

The behavior of single piles (monopiles) under lateral loading has been extensively studied over the four last decades. The researchers found out that the key element of the behavior of these

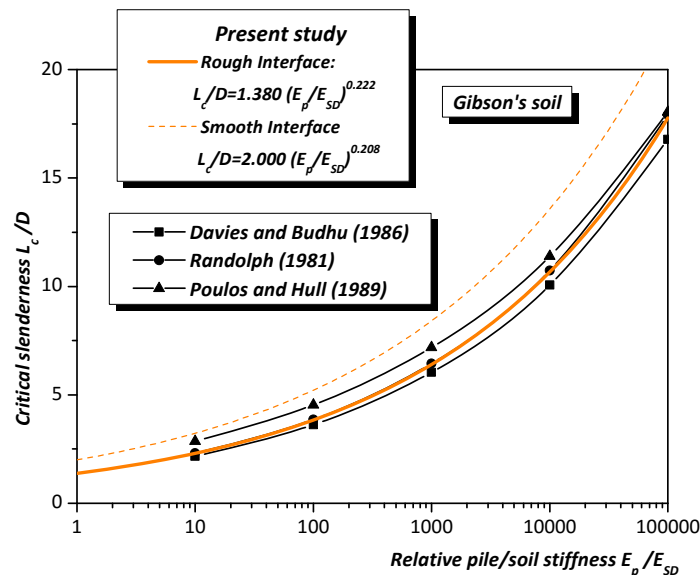
foundations is what we call the critical length or the critical slenderness (Banerjee and Davies 1978, Poulos and Davis 1980, Randolph 1981, Gazetas 1991). This parameter really separates the behavior of long slender monopiles than that of short piles. In slender monopiles the head movements cease to be dependent on the pile length when this length is greater than its critical length. However, short monopiles behave differently and depend on contrary on monopile length.

As there is a dearth of research studies for problems where the interface between the soil and the monopile is smooth or the soil considered has a stiffness which varies as a square root of depth, this section is dedicated to find finite element expressions of critical slenderness. Indeed, the procedure followed is to set up the soil stiffness $E_s(z) = E_{SD}(z/D_p)^\alpha$ at a fixed value and to increment the slenderness ratio. The procedure terminates when a convergence criterion reaches a pre-set limit. In other words the procedure stops when the increase in the monopile length cease to have an effect on the head movements. Table 2 gives the different expressions for monopile slenderness.

These expressions as well as existing solutions found in the literature are illustrated in the Fig. 9. It is clear from a close examination of these Figures that the effect of interface state is not important for a soil with a parabolic variation of stiffness with depth.

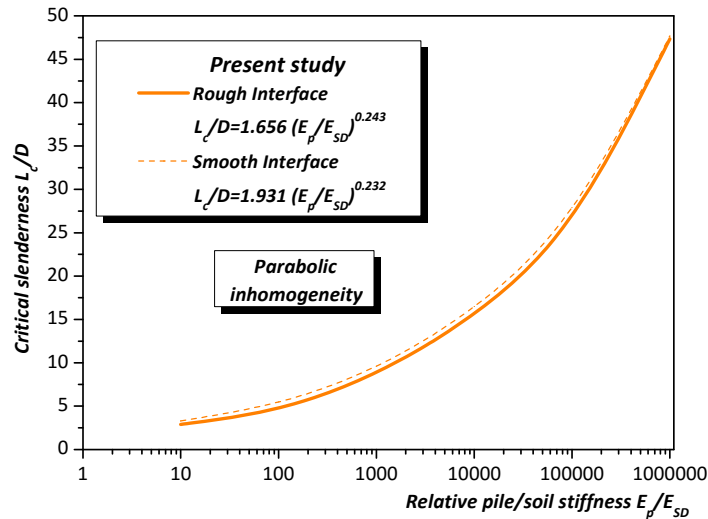
Table 2 Expressions of slenderness ratios for a monopile embedded in different soil profiles

Soil profile	Rough interface	Smooth interface
Gibson's soil	$L_c/D = 1.380(E_p/E_{SD})^{0.222}$	$L_c/D = 2.000(E_p/E_{SD})^{0.208}$
Parabolic variation of stiffness	$L_c/D = 1.656(E_p/E_{SD})^{0.243}$	$L_c/D = 1.931(E_p/E_{SD})^{0.232}$



(a)

Fig. 9 Evolution of critical slenderness L_c/D with E_p/E_{SD} for monopile embedded in different soil profiles: (a) Gibson's, and (b) parabolic non-homogeneity



(b)

Fig. 9 Continued

Expressions of Table 2 are used to show the limit between the stiff and the flexible monopiles in the Figs. 10-17.

5.2 Existing solutions for slender monopiles

The monopile under lateral loading is marked by its head movements. Indeed, monopile head lateral displacement and monopile head rotation are of paramount importance in predicting monopile behavior. Head movements and applied efforts are usually expressed through the flexibility factors according to the following relationships

$$\begin{Bmatrix} u_L \\ \theta_R \end{Bmatrix} = \begin{bmatrix} I_L & I_{LR} \\ I_{RL} & I_R \end{bmatrix} \begin{Bmatrix} H \\ M \end{Bmatrix} \tag{20}$$

Expressions in which, $I_{LR} = I_{RL}$ according to Maxwelli-Betti principle. In engineering practice the inverse of the matrix (20) is practically more important. It has the following form

$$\begin{Bmatrix} H \\ M \end{Bmatrix} = \begin{bmatrix} K_L & K_{LR} \\ K_{RL} & K_R \end{bmatrix} \begin{Bmatrix} u_L \\ \theta_R \end{Bmatrix} \tag{21}$$

The stiffness coefficients appearing in matrix Eq. (21) are related to the flexibility coefficients of Eq. (20) by the following expressions

$$K_H = \frac{I_M}{I_H I_M - I_{MH}^2}, \quad K_M = \frac{I_H}{I_H I_M - I_{MH}^2}, \quad K_{MH} = \frac{I_{MH}}{I_H I_M - I_{MH}^2} \tag{22}$$

In the finite element analyses controlled by forces, the determination of the head stiffness coefficients is not straightforward. The flexibility coefficients are determined first, and then

Table 3 Stiffness coefficients for slender piles proposed by different authors in Gibson’s soil

No.	Authors	Horizontal stiffness coefficient $K_L/E_{sD}D$	Coupling stiffness coefficient $K_{LR}/E_{sD}D^2 = K_{RL}/E_{sD}D^2$	Rocking stiffness coefficient $K_R/E_{sD}D^3$
01	Randolph 1981	$1.751(E_p/E_{sD})^{0.333}$	$-0.506(E_p/E_{sD})^{0.555}$	$0.248(E_p/E_{sD})^{0.777}$
02	Davies and Budhu 1986	$0.734(E_p/E_{sD})^{0.333}$	$-0.270(E_p/E_{sD})^{0.555}$	$0.173(E_p/E_{sD})^{0.777}$
03	Amar Bouzid 1997	$1.138(E_p/E_{sD})^{0.327}$	$-0.591(E_p/E_{sD})^{0.523}$	$0.450(E_p/E_{sD})^{0.726}$
04	DNV/RISØ 2004	$0.600(E_p/E_{sD})^{0.350}$	$-0.170(E_p/E_{sD})^{0.600}$	$0.140(E_p/E_{sD})^{0.800}$

inversed to obtain the stiffness coefficients of Eq. (22).

Most researchers found out that the monopile head movements depend on monopile/soil stiffness (E_p/E_s or E_p/G_s) and presented closed form solutions for flexibility coefficients. Table 3 presents expressions proposed by different authors for slender monopiles embedded in Gibson’s soil. These values have been obtained by inverting the flexibility matrix and presented properly according to the expressions of soil modulus adopted in this paper.

5.3 Development of static impedance functions for short monopiles

Studies dealing with short monopiles are scarce in the literature. Higgins *et al.* (2013) presented closed form solutions for flexibility factors I_L , I_R and I_{LR} for monopiles embedded in both homogeneous and Gibson’s soils. As the sum of the powers included in the expressions of I_L and I_R does not correspond to two times the power included in the expression of I_{LR} , straightforward closed form solutions for the stiffness coefficients K_L , K_R and K_{LR} are difficult to obtain. However the inversion of the flexibility factors at discrete values of (L_p/D_p) is easy to carry out. Then, analytical expressions were found as best fits of the obtained results. Table 4 shows the stiffness coefficients for short monopiles obtained from flexibility factors proposed by Higgins *et al.* (2013).

These expressions are used for comparison with the results issued from the numerical procedure in this study.

In order to develop static impedance functions for monopiles embedded in two soil profiles, namely, Gibson’s and a soil in which the soil modulus varies as a square root of depth, an extensive parametric study has been carried out. In order to cover a wide range of short monopiles,

Table 4 Stiffness coefficients for short monopiles proposed by Higgins *et al.* (2013) for Gibson’s soils

Authors	Soil nature	Poisson’s ratio ν_s	Horizontal stiffness coefficient $K_L/E_{sD}D$	Coupling stiffness coefficient $K_{LR}/E_{sD}D^2 = K_{RL}/E_{sD}D^2$	Rocking stiffness coefficient $K_R/E_{sD}D^3$
Higgins <i>et al.</i> (2013)	Gibson’s	0.40	$0.929 (L_p/D_p)^{2.041}$	$-0.633 (L_p/D_p)^{3.061}$	$0.672 (L_p/D_p)^{3.941}$
		0.499	$0.916 (L_p/D_p)^{2.041}$	$-0.624 (L_p/D_p)^{3.061}$	$0.662 (L_p/D_p)^{3.941}$

six (06) slenderness ratios were chosen namely: $L_p/D_p = 1, 2, 4, 6, 10$ and 15 with six (06) soil/pile relative stiffnesses which are: $E_p/E_{SD} = 10, 10^2, 10^3, 10^4, 10^5$ and 10^6 . Finite element results are presented for two (02) Poisson's ratios $\nu_s = 0.40$ and $\nu_s = 0.499$.

It has been found that the monopile head movements (lateral displacement and head rotations) are independent of the modulus ratio (E_p/E_{SD}), and depend only on the slenderness ratio (L_p/D_p) and Poisson's ratio of the soil mass (ν_s).

Lateral stiffness coefficient K_L , rocking stiffness K_R and cross coupling stiffness coefficient K_{LR} for monopiles embedded in a Gibson's soil with a rough interface and soil Poisson's ratio $\nu_s = 0.40$ and Poisson's ratio $\nu_s = 0.499$ are respectively presented in Figs. 10 and 11. Also shown, is a comparison between finite element results and those provided by Higgins *et al.* (2013) for Gibson's soil.

A close examination of these Figures shows two interesting features. Firstly, the analytical expressions of the static impedance functions which appear in the Figs. 10 and 11, are sufficiently accurate as they match the results envelope. These approximate equations are

$$K_L = 1.708 E_{SD} D_p (L_p/D_p)^{1.661}$$

$$K_R = 1.153 E_{SD} D_p^3 (L_p/D_p)^{3.605} \quad \text{For } \nu_s = 0.40 \quad (23)$$

$$K_{LR} = -1.233 E_{SD} D_p^2 (L_p/D_p)^{2.655}$$

$$K_L = 1.647 E_{SD} D_p (L_p/D_p)^{1.694}$$

$$K_R = 1.115 E_{SD} D_p^3 (L_p/D_p)^{3.633} \quad \text{For } \nu_s = 0.499 \quad (24)$$

$$K_{LR} = -1.189 E_{SD} D_p^2 (L_p/D_p)^{2.687}$$

Secondly, an excellent agreement is observed between FSAFEM results and those obtained by Higgins *et al.* (2013) for the range of slenderness ratios up to 6, and a discrepancy occurred in the remaining interval of slendernesses considered in this study and for both figures.

K_L , K_R and K_{LR} for monopiles embedded in a Gibson's soil with a smooth interface and soil Poisson's ratio $\nu_s = 0.40$ and Poisson's ratio $\nu_s = 0.499$ are respectively reported in Figs. 12 and 13.

For simulating smooth interface, FE analyses were carried out by imposing a shear stiffness of $k_s = 0.0$ and a large value for the normal stiffness for k_n , for instance $k_n = 10^{12} \text{ kN/m}^3$. The obtained formulae for this case are

$$K_L = 1.259 E_{SD} D_p (L_p/D_p)^{1.720}$$

$$K_R = 0.813 E_{SD} D_p^3 (L_p/D_p)^{3.672} \quad \text{For } \nu_s = 0.40 \quad (25)$$

$$K_{LR} = -0.914 E_{SD} D_p^2 (L_p/D_p)^{2.709}$$

$$K_L = 1.214 E_{SD} D_p (L_p/D_p)^{1.748}$$

$$K_R = 0.815 E_{SD} D_p^3 (L_p/D_p)^{3.686} \quad \text{For } \nu_s = 0.499 \quad (26)$$

$$K_{LR} = -0.897 E_{SD} D_p^2 (L_p/D_p)^{2.732}$$

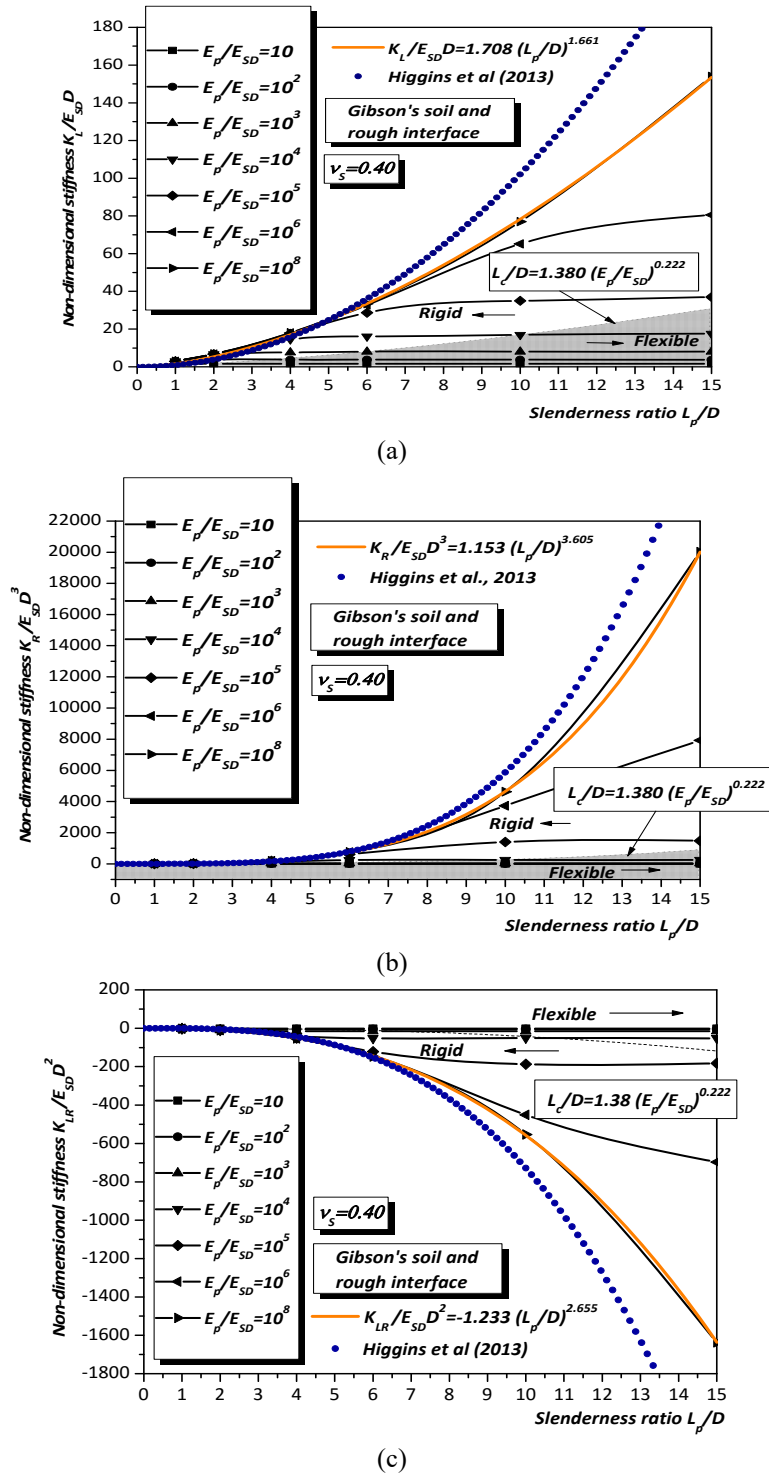
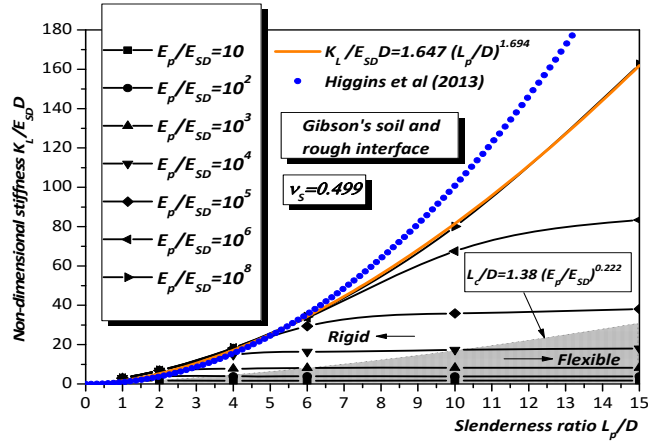
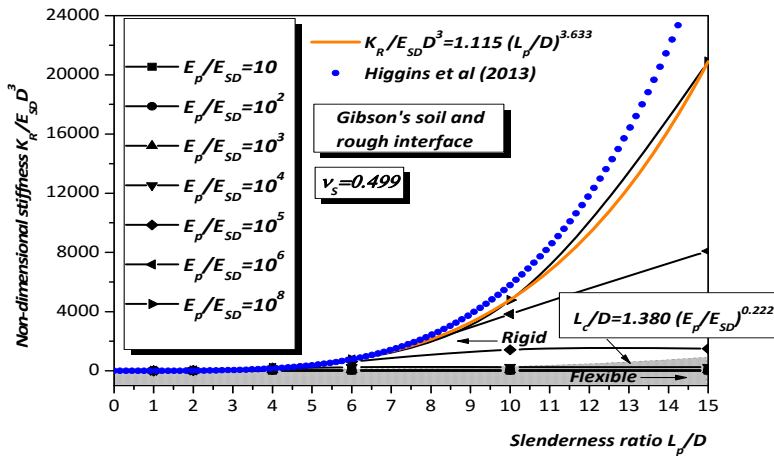


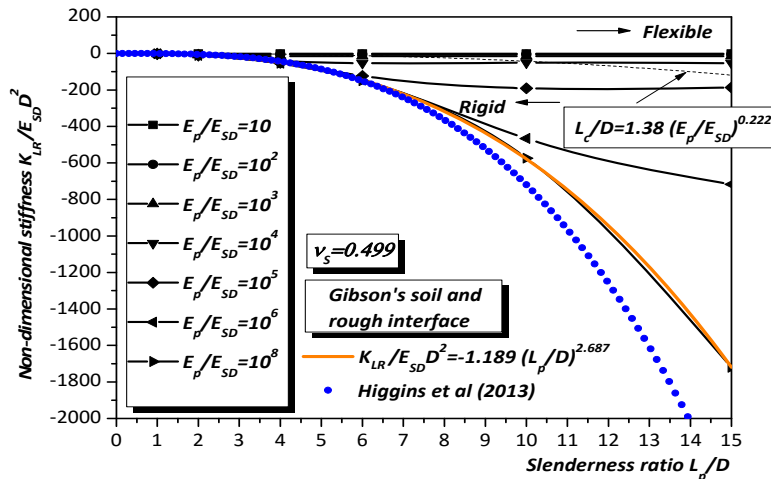
Fig. 10 Stiffness coefficients, (a) K_L , (b) K_R and (c) K_{LR} for piles embedded in a Gibson's soil with a rough interface and soil Poisson's ratio $\nu_s = 0.40$



(a)



(b)



(c)

Fig. 11 Stiffness coefficients, (a) K_L , (b) K_R and (c) K_{LR} for piles embedded in a Gibson's soil with a rough interface and soil Poisson's ratio $v_s = 0.499$

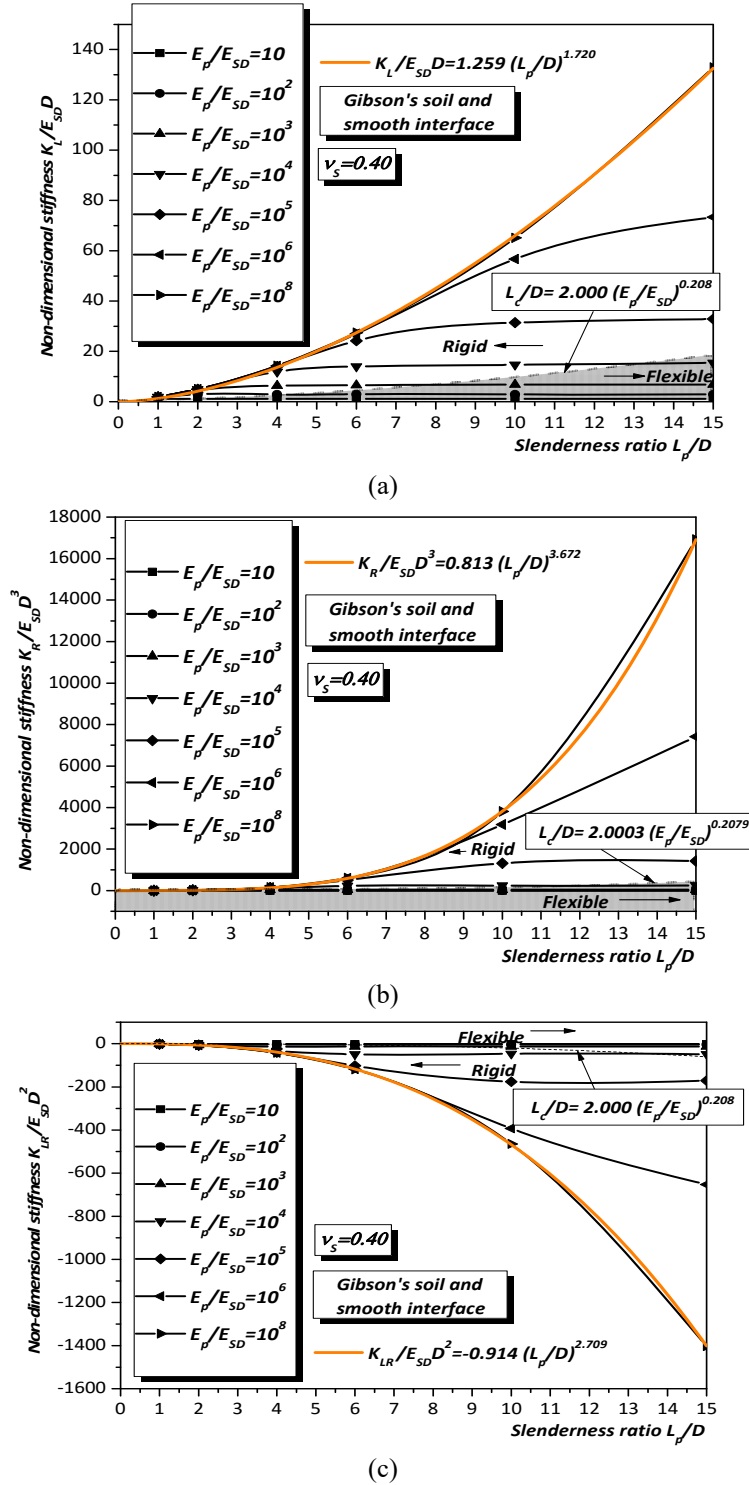


Fig. 12 Stiffness coefficients, (a) K_L , (b) K_R and (c) K_{LR} for piles embedded in a Gibson's soil with a smooth interface and soil Poisson's ratio $\nu_s = 0.40$

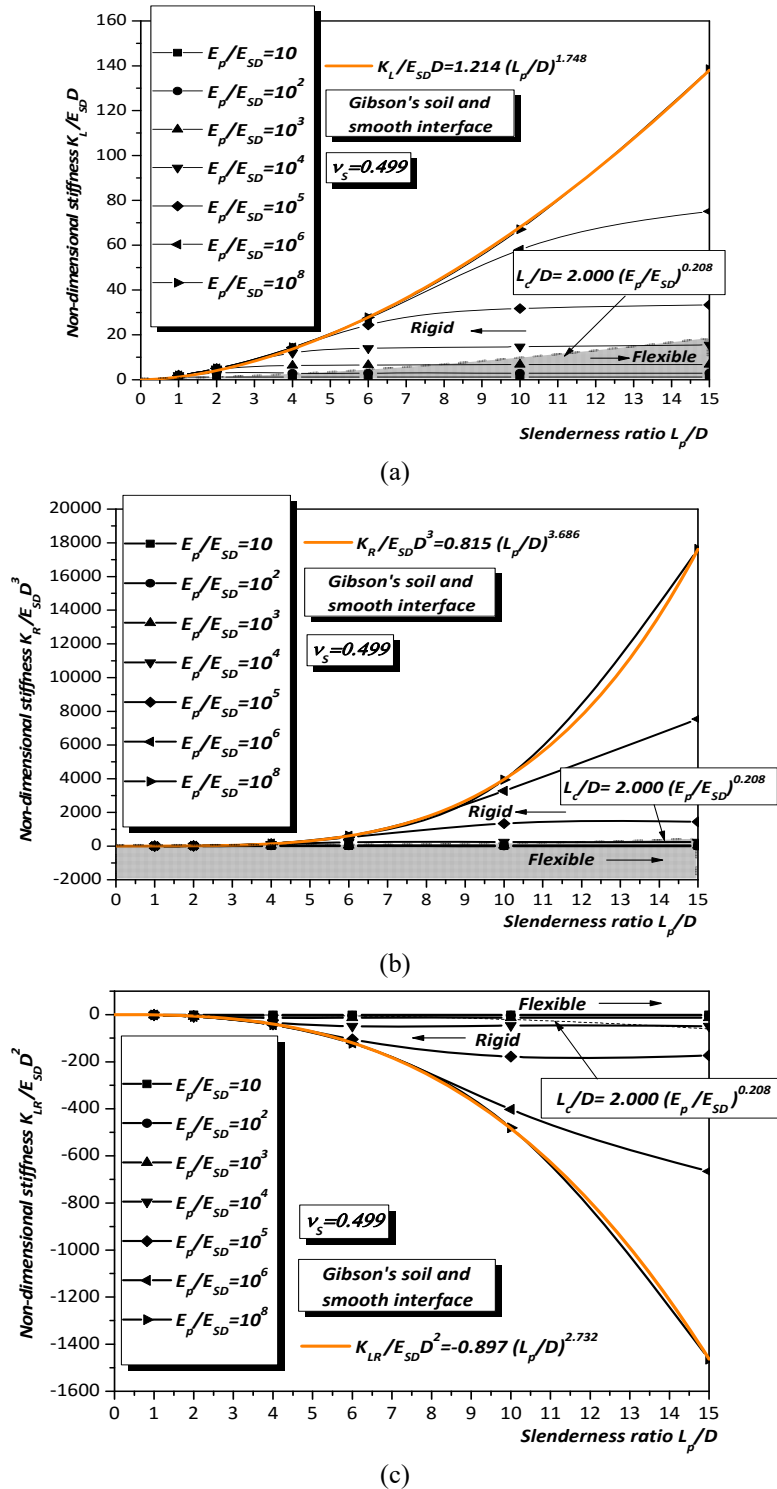
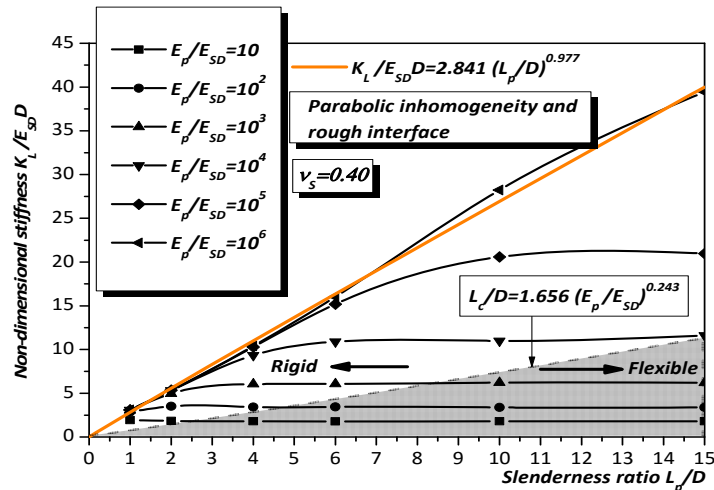


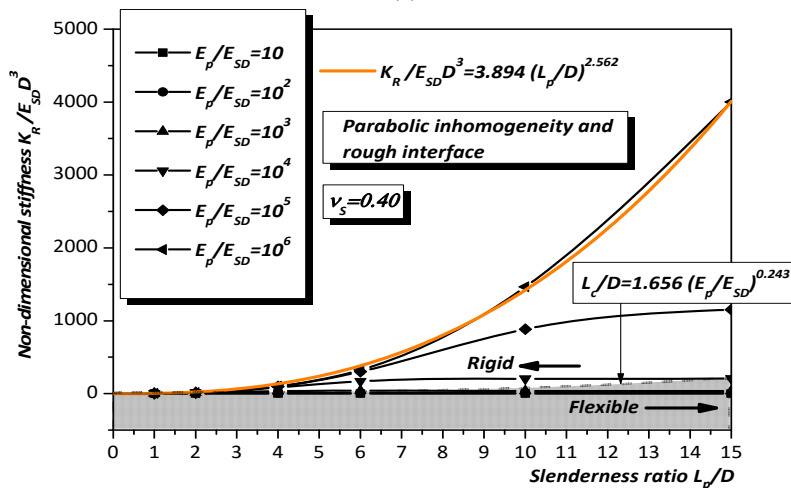
Fig. 13 Stiffness coefficients, (a) K_L , (b) K_R and (c) K_{LR} for piles embedded in a Gibson's soil with a smooth interface and soil Poisson's ratio $\nu_s = 0.499$

Three points emerge from the consideration of Figs. 12 and 13. Firstly, K_L , K_R and K_{LR} are much lower than their corresponding values in the case of rough interface. Secondly, expressions obtained in this case can be used as lower bound of stiffness coefficient for the calculation of monopile head movements. Thirdly, for most practical applications values of K_L , K_R and K_{LR} range between the expressions obtained when the rough interface is considered and the smooth one.

Figs. 14 and 15 illustrate the evolution of K_L , K_R and K_{LR} with the slenderness ratio (L_p/D_p) for monopiles embedded in a soil where the stiffness varies as a square root of depth, with a rough interface and soil Poisson's ratio $\nu_s = 0.40$ and Poisson's ratio $\nu_s = 0.499$ respectively. The approximate expressions obtained are

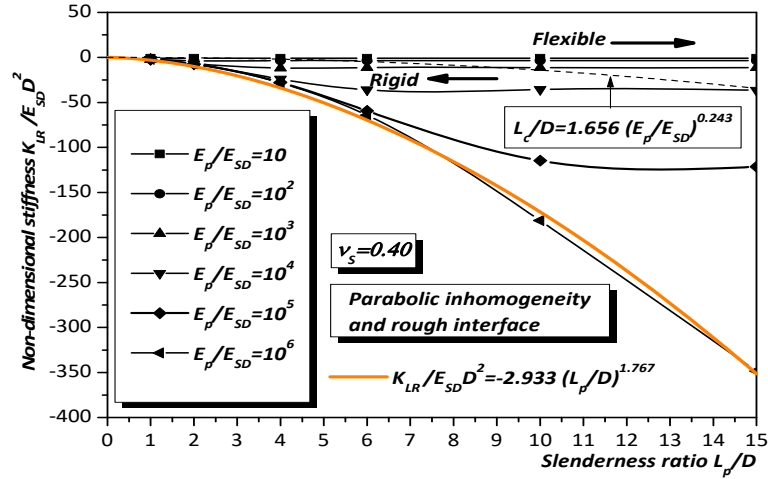


(a)



(b)

Fig. 14 Stiffness coefficients, (a) K_L , (b) K_R and (c) K_{LR} for piles embedded in a soil characterized by parabolic inhomogeneity with a rough interface and soil Poisson's ratio $\nu_s = 0.40$



(c)

Fig. 14 Continued

$$K_L = 2.841 E_{SD} D_p (L_p / D_p)^{0.977}$$

$$K_R = 3.894 E_{SD} D_p^3 (L_p / D_p)^{2.562} \quad \text{For } \nu_s = 0.40 \quad (27)$$

$$K_{LR} = -2.933 E_{SD} D_p^2 (L_p / D_p)^{1.767}$$

$$K_L = 2.830 E_{SD} D_p (L_p / D_p)^{0.996}$$

$$K_R = 3.937 E_{SD} D_p^3 (L_p / D_p)^{2.571} \quad \text{For } \nu_s = 0.499 \quad (28)$$

$$K_{LR} = -2.942 E_{SD} D_p^2 (L_p / D_p)^{1.782}$$

The variation of the head monopile stiffness coefficients with the slenderness ratio when a smooth interface is considered is presented in Figs. 16 and 17. The analytical expressions for K_L , K_R and K_{LR} are given by Eqs. (29) and (30)

$$K_L = 2.081 E_{SD} D_p (L_p / D_p)^{1.050}$$

$$K_R = 2.451 E_{SD} D_p^3 (L_p / D_p)^{2.690} \quad \text{For } \nu_s = 0.40 \quad (29)$$

$$K_{LR} = -2.067 E_{SD} D_p^2 (L_p / D_p)^{1.857}$$

$$K_L = 2.055 E_{SD} D_p (L_p / D_p)^{1.067}$$

$$K_R = 2.555 E_{SD} D_p^3 (L_p / D_p)^{2.686} \quad \text{For } \nu_s = 0.499 \quad (30)$$

$$K_{LR} = -2.100 E_{SD} D_p^2 (L_p / D_p)^{1.865}$$

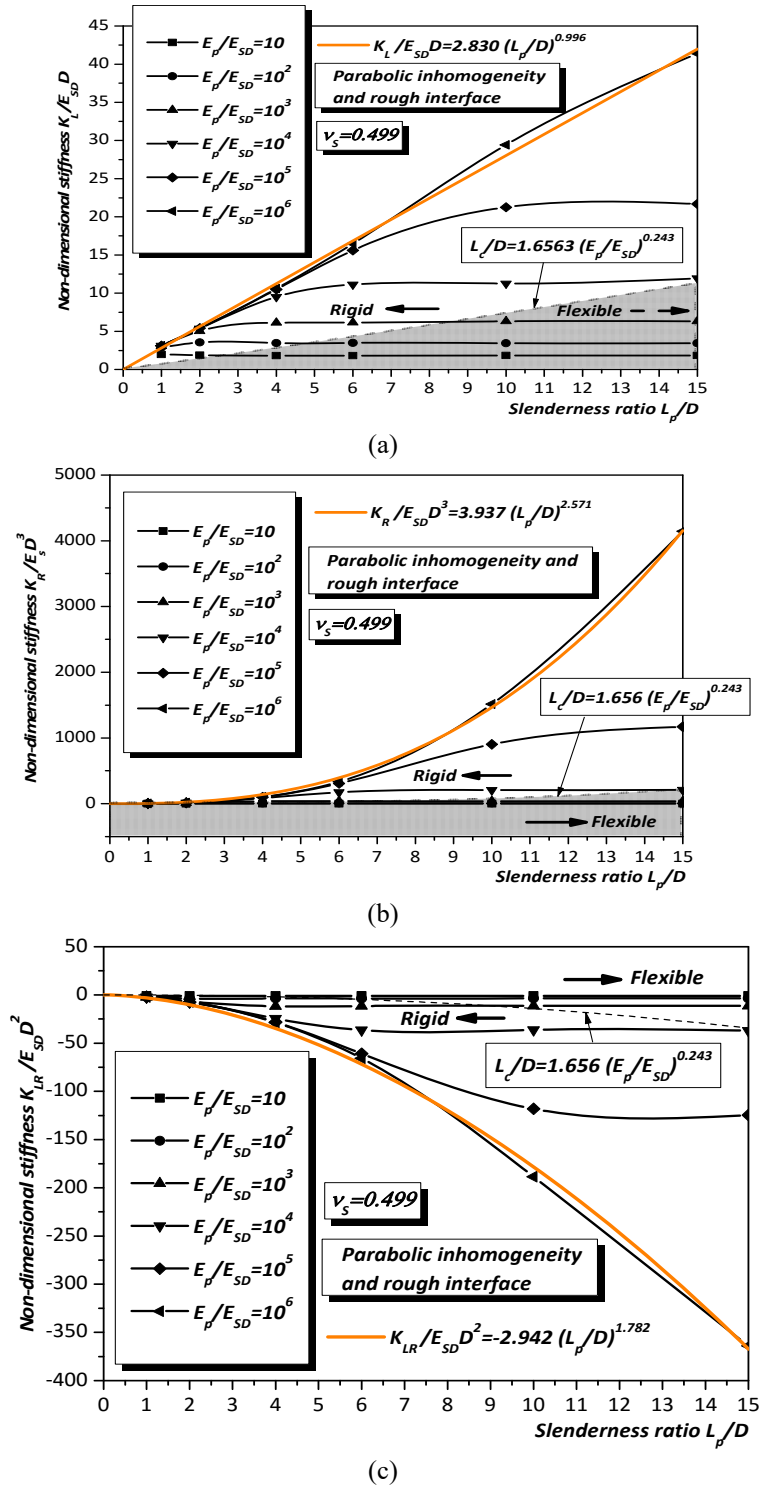


Fig. 15 Stiffness coefficients, (a) K_L , (b) K_R and (c) K_{LR} for piles embedded in a soil characterized by parabolic inhomogeneity with a rough interface and soil Poisson's ratio $\nu_s = 0.499$

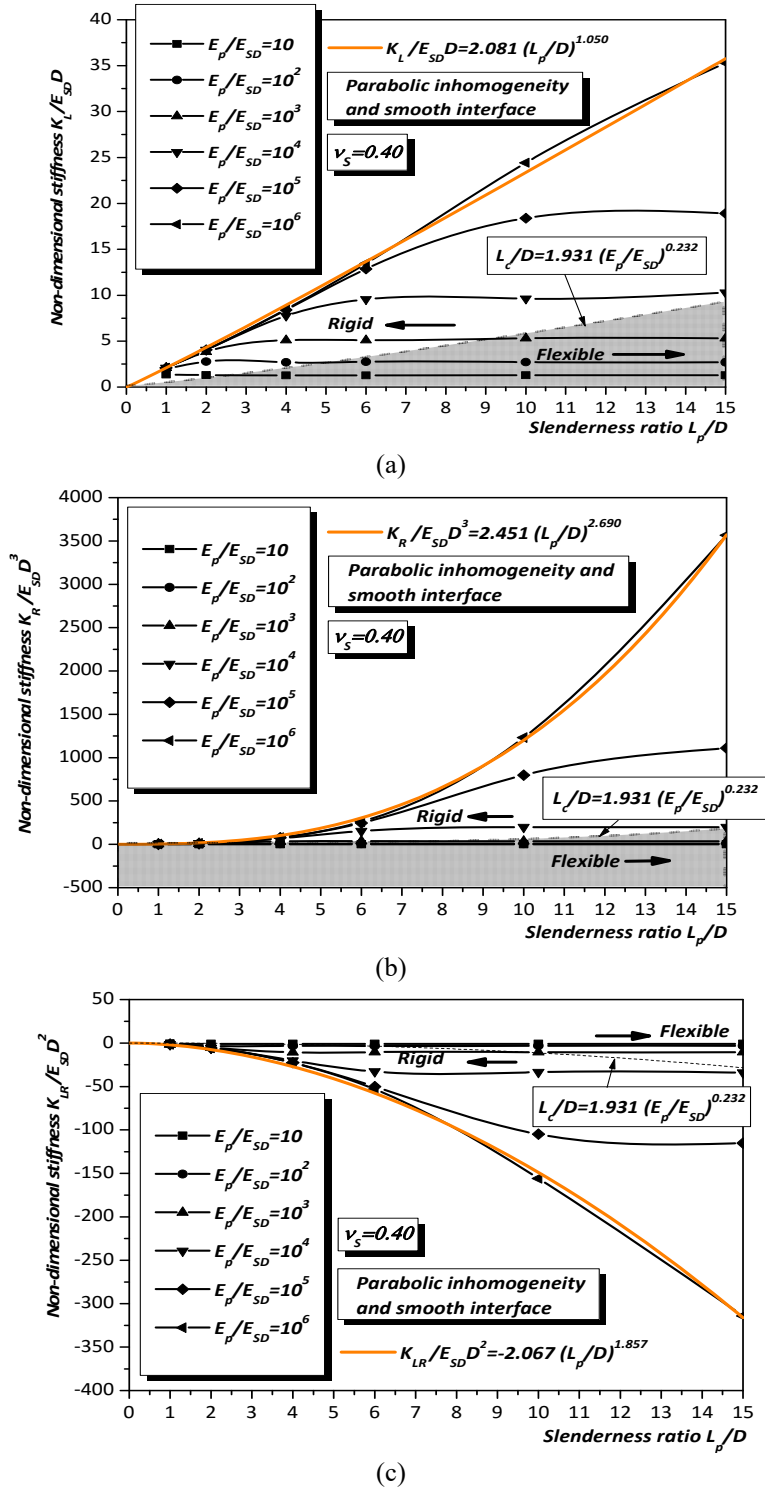


Fig. 16 Stiffness coefficients, (a) K_L , (b) K_R and (c) K_{LR} for piles embedded in a soil characterized by parabolic inhomogeneity with a smooth interface and soil Poisson's ratio $\nu_s = 0.40$

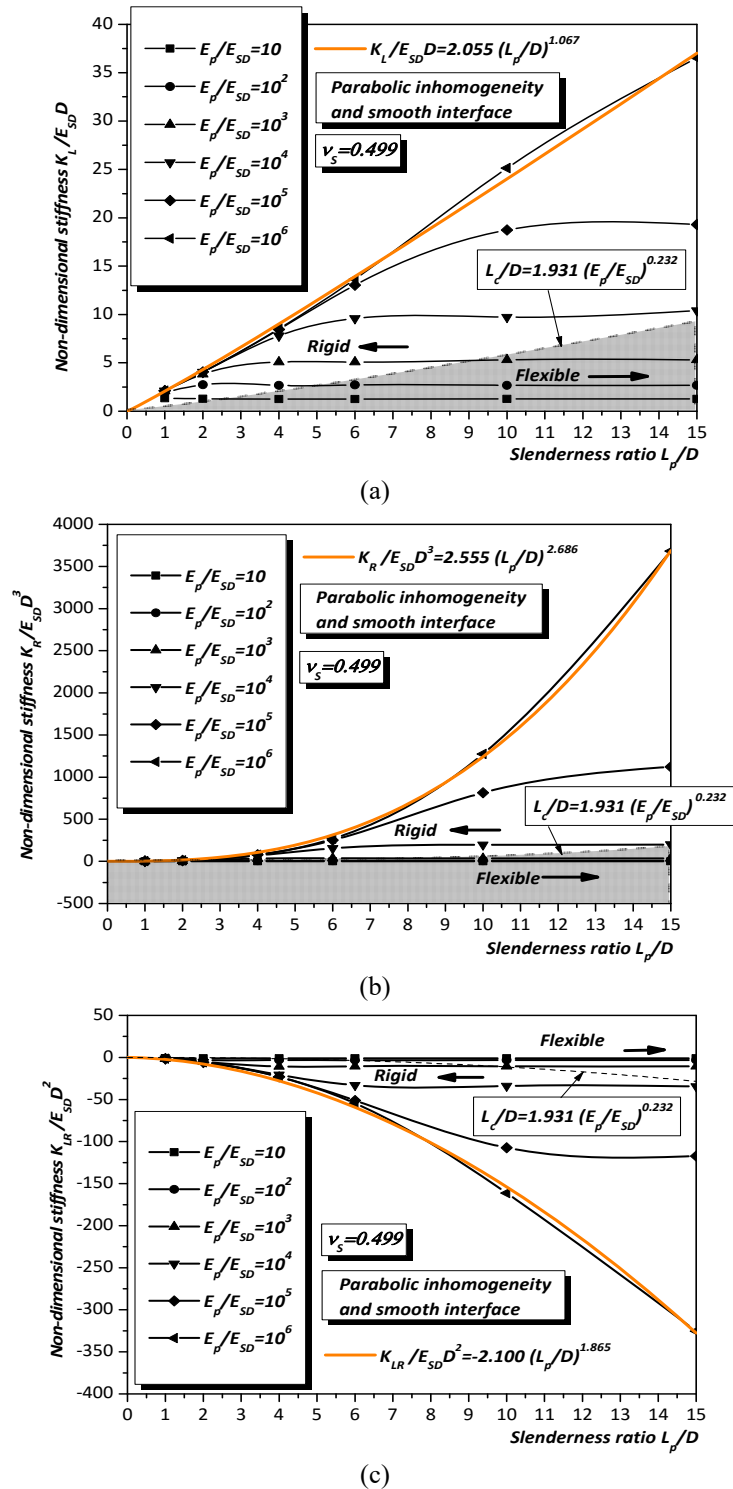


Fig. 17 Stiffness coefficients, (a) K_L , (b) K_R and (c) K_{LR} for piles embedded in a soil characterized by parabolic inhomogeneity with a smooth interface and soil Poisson's ratio $\nu_s = 0.499$

6. Dynamics of wind turbines considering soil-structure interaction

Offshore wind turbines can be considered as high slenderness low stiffness dynamical system involving complex interaction between the wind, wave and the soil. Consequently, the behavior of an offshore wind turbine as well as its substructure are significantly affected by the determination of the first natural frequency.

Offshore wind turbines are dynamically sensitive structures that are placed in harsh environmental conditions, with strong wind and wave loading of a cyclic nature. This makes the design of foundations extremely challenging (Lombardi *et al.* 2013, Damgaard *et al.* 2014, Damgaard *et al.* 2015, Meyers *et al.* 2015).

The design of the structure and the substructure of an offshore wind turbine should be carried out in such a way that it sustains the permanent dynamic forces induced by vibrations during its operational life. These forces with the combination of the operating frequency could potentially trigger the resonance phenomenon. This can have catastrophic consequences and needs to be avoided at all costs. The main sources of excitation are wind and waves as an offshore wind turbine is in a permanent interaction with two media: air and water. On one hand, the waves generating the excitation, are relatively short waves with a significant wave height H_s around 1-1.5 m and a zero-crossing period T_z around 4-5 s. This excitation is shown in Fig. 18. On the other hand, the excitations generated by wind are the frequencies that are close to the rotational frequencies of the rotor $1P$ and the blade passing frequency (The blade/tower interaction), which relies on the number of blades. As most turbines existing in the market have 3 blades therefore it is $3P$. The natural frequency needs to be chosen to avoid these frequencies. The targeted region is the one illustrated in the Fig. 18. Moreover the wind turbulence also causes excitations also plotted along with the other frequencies.

To avoid resonance which may lead to the failure, the OWT should be designed such that the first natural frequency should lie between turbine and blade passing frequencies, i.e., in the interval corresponding to the “Soft-Stiff” interval in Fig. 18.

The region before the $1P$ is called the “Soft-Soft” region while the region after the $3P$ is known as “Stiff-Stiff” region. If the natural frequency of the design lies in the Soft-Soft interval it will be too flexible while in the Stiff-Stiff region it will be too rigid (Heavy/Expensive), making it inappropriate for the design. As evident from Fig. 18 the “Soft-Soft” usually contains the wave

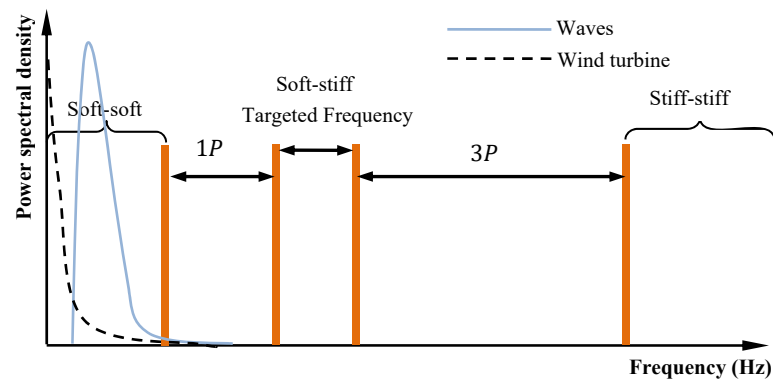


Fig. 18 Excitation intervals of a three-bladed offshore wind turbine

and wind turbulence excitation frequencies this is another reason why this region is usually avoided.

6.1 Natural frequency as a function the monopile head stiffnesses

Estimating the first natural frequency of an OWT, is not an easy work, as it depends on an accurate modeling of the structure as well as the monopile foundation which is involved in an extremely complex subsoil/monopile interaction problem (Jin-Hak *et al.* 2015, Prendergast *et al.* 2015, Andersen *et al.* 2012, Al Hamaydeh and Hussain 2011). Many authors had focused their work on this issue. Indeed, Vught (2000) modeled the wind turbine as a flagpole of length L , mass per length m , top mass M and having an average bending stiffness EI . His expression for the first natural frequency is

$$f_1 \cong \sqrt{\frac{3.04EI}{(M+0.227 mL)4\pi^2L^3}} \tag{31}$$

Although simple, it seems from the very first look to this equation that the OWT is embedded in a medium having an infinite stiffness. This is unrealistic, as the system monopile/subsoil is characterized by a certain flexibility which has an effect on the value of the first natural frequency.

The first natural frequency is closely related to the behavior of both tower and substructure of the wind turbine. Hence, the accurate modeling of this problem, should consider the monopile head stiffnesses determined by Eqs. (23)-(30) as spring stiffnesses through which the tower is connected to the subsoil. Fig. 19 shows a mechanical model, in which the foundation is represented by four springs, a lateral, a rocking, a cross-coupling and a vertical spring. As the wind turbines are very stiff vertically the axial vibrations can be neglected.

Adhikari and Bhattacharya (2011) proposed an exact approach based on a numerical solution of transcendental frequency equation. The latter depends only on lateral and rotational stiffnesses.

In order to further enhance the first natural frequency equation, Laszlo *et al.* (2014) proposed an analytical expression encompassing the cross coupling stiffness of the monopile. The natural frequency of the wind turbine proposed is

$$f_\eta = C_R C_L f_{FB} \tag{32}$$

Where f_{FB} is the fixed base frequency given by

$$f_{FB} = \frac{1}{2\pi} \sqrt{\frac{3EI\eta}{(M_{top} + \frac{33}{140}ML_{tower})L_{tower}^3}} \tag{33}$$

Eq. (33) which has been proposed by Tempel and Molenaar (2002) is used in this paper. It differs slightly from the Eq. (31), which corresponds also to a fixed base. Expressions for $C_R(\eta_L, \eta_R, \eta_{LR})$ and $C_L(\eta_L, \eta_R, \eta_{LR})$ are given by

$$C_R(\eta_L, \eta_R, \eta_{LR}) = 1 - \frac{1}{1+a\left(\eta_R - \frac{\eta_{LR}^2}{\eta_L}\right)} \tag{34}$$

$$C_L(\eta_L, \eta_R, \eta_{LR}) = 1 - \frac{1}{1+b\left(\eta_L - \frac{\eta_{LR}^2}{\eta_R}\right)} \tag{35}$$

The parameters involved in the expressions (34) and (35) are grouped in Table 5.

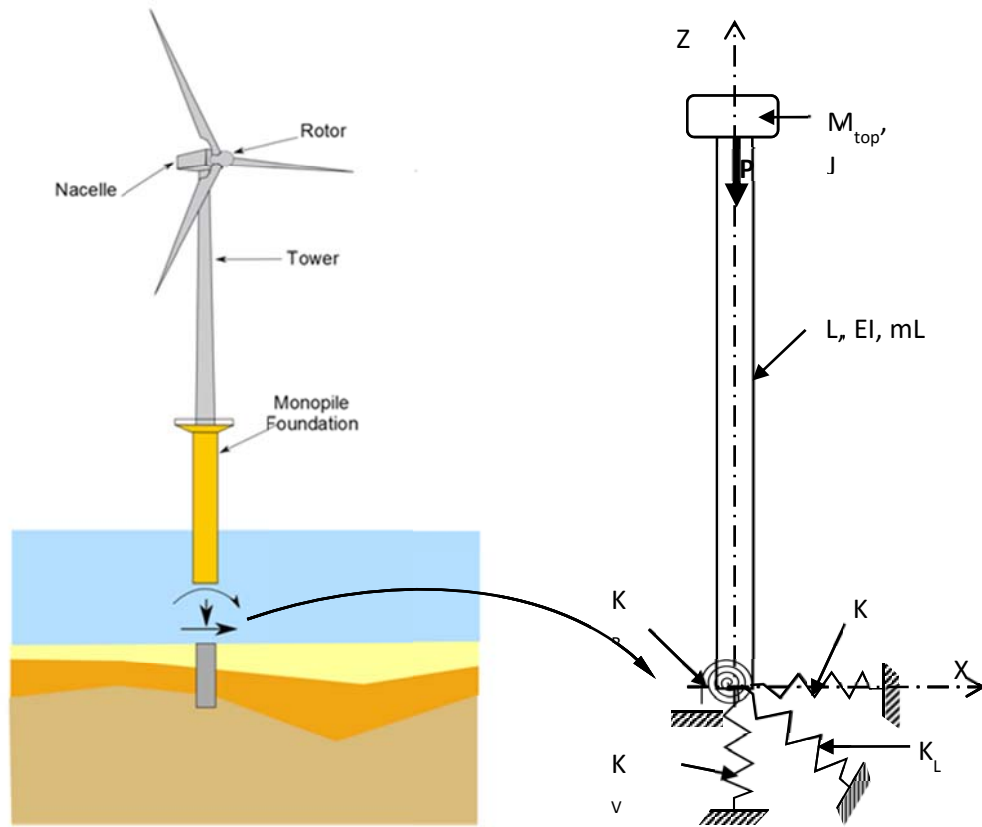


Fig. 19 Wind turbine model

Table 5 Non-dimensional expressions

η_L	η_R	η_{LR}	a	b
$(K_L L^3_{tower})/EI_\eta$	$(K_R L_{tower})/EI_\eta$	$(K_{LR} L^2_{tower})/EI_\eta$	0.6	0.5

6.2 Verification of natural frequency prediction for four different wind turbines

In order to validate the different expressions found for the short monopiles, and in order to illustrate the accuracy, utility and potential of the proposed method, four (04) wind farm sites have been chosen from the literature namely: Lely A2 (UK), North Hoyle (The Netherlands), Irene Vorrink (The Netherlands), and Walney 1 (UK). The turbines data and the sites characteristics are summarized in Table 6.

As the fixed base natural frequency depends only on the tower properties, it is computed first. Its values for the different sites are given in Table 7.

For lack of information, the Poisson’s ratio has been taken 0.40 for all turbines considered in this paper. Consequently the expressions used for the computation of the monopile head stiffnesses are the Eqs. (23), (25), (27) and (29). They are grouped in Table 8.

Table 6 Turbine data for the four wind farms chosen for this study

WIND FARM SITE NAME	LELY A2	NORTH HOYLE	IRENE VORRINK	WALNEY 1
TURBINE DATA				
Turbine type	NM41	Vestas V80	NTK 600	Siemens SWT
Turbine power (Kw)	500	2×10 ³	600	(3.6-107.63)×10 ³
Turbine rotor diameter (m)	40.77	80	43	107
Turbine rotational speed (rpm)	32	10.8-19.1	27	5-13
Operational wind speed range (m/s)	4.0	4.0	4.0	4.25
TOWER DATA				
Tower height (m)	41.5	70	51	83.5
Tower top diameter (m)	1.9	2.3	1.7	3
Tower bottom diameter (m)	3.2	4.0	3.5	5
Tower wall thickness (mm)	12	35	8-14	40 (average)
Tower material young's (GPa) modulus	210.0	210.0	210.0	210.0
Tower mass (Kg)	31346.0	130000.0	35700.0	260000.0
Top mass(Kg)	32000.0	100000.0	34000.0	236000.0
PILE DATA				
Pile diameter (m)	3.7	4	3.5	6
Pile wall thickness (mm)	35	50	28	80
Pile material young's modulus (Gpa)	210	210	210	210
Pile depth (m)	20.9	33	19	23.5
SOIL DATA				
Soil type	Soft to stiffer sandy layer	Sand and clay layers	Stiffer sandy soil	Clay on top, sand below
Shear modulus of the soil (Mpa)	53	230	55	70
Poisson's ratio of the soil	0.4	0.4	0.4	0.4
FREQUENCY				
Measured frequency (Hz)	0.634	0.35	0.546-0.56	0.35

Table 7 Fixed base natural frequency for each site

Wind farm site	WALNEY 1	LELY A2	NORTH HOYLE	IRENE VORRINK
f_{FB} (Hz)	0.347	0.768	0.448	0.552

The following Tables summarize the different steps of computations when a linear or a parabolic variation of soil stiffness with depth, are considered. Using expressions tabulated in Table 8, the computed values for K_L , K_R and K_{LR} for the different wind farm sites are grouped in Tables 9 and 10.

Table 8 Monopile head stiffness expressions

Soil profiles	Interface	K_L	K_R	K_{LR}
Gibson's	Rough	$1.708 E_{SD} D_p (L_p/D_p)^{1.661}$	$1.153 E_{SD} D_p^3 (L_p/D_p)^{3.605}$	$-1.233 E_{SD} D_p^2 (L_p/D_p)^{2.655}$
	Smooth	$1.259 E_{SD} D_p (L_p/D_p)^{1.720}$	$0.813 E_{SD} D_p^3 (L_p/D_p)^{3.672}$	$-0.914 E_{SD} D_p^2 (L_p/D_p)^{2.709}$
Parabolic variation	Rough	$2.841 E_{SD} D_p (L_p/D_p)^{0.977}$	$3.894 E_{SD} D_p^3 (L_p/D_p)^{2.562}$	$-2.933 E_{SD} D_p^2 (L_p/D_p)^{1.767}$
	Smooth	$2.081 E_{SD} D_p (L_p/D_p)^{1.050}$	$2.451 E_{SD} D_p^3 (L_p/D_p)^{2.690}$	$-2.067 E_{SD} D_p^2 (L_p/D_p)^{1.857}$

Table 9 Monopile head stiffness values for Walney 1 and Lely A2 wind farm sites

Soil profiles	Interface	WALNEY 1			LELY A2		
		$K_L(GN/m)$	$K_R(GN.m/rad)$	$K_{LR}(GN)$	$K_L(GN/m)$	$K_R(GN.m/rad)$	$K_{LR}(GN)$
Gibson's	Rough	19.397	6699.061	-326.578	16.639	4452.369	-248.627
	Smooth	15.489	5171.286	-260.295	13.574	3522.335	-202.085
Parabolic variation	Rough	12.674	5445.198	-231.064	8.461	2470.158	-127.075
	Smooth	10.266	4082.849	-184.206	7.041	1941.233	-104.707

Table 10 Monopile head stiffness values for North Hoyle and Irene Vorrink wind farm sites

Soil profiles	Interface	NORTH HOYLE			IRENE VORRINK		
		$K_L(GN/m)$	$K_R(GN.m/rad)$	$K_{LR}(GN)$	$K_L(GN/m)$	$K_R(GN.m/rad)$	$K_{LR}(GN)$
Gibson's	Rough	146.455	95636.789	-3447.910	15.290	3388.936	-207.749
	Smooth	122.163	77604.449	-2859.855	12.445	2673.909	-168.501
Parabolic variation	Rough	57.472	35741.709	-1258.829	7.990	1959.739	-109.996
	Smooth	49.172	29487.288	-1073.303	6.629	1532.275	90.310

Table 11 Equivalent flexural rigidity for the different wind towers considered in this paper.

Wind farm	m	$f_p(m)$	$(EI)_{top} (GN \times m^2)$	$EI_\eta (GN \times m^2)$
Walney 1	1.667	3.204	85.564	274.149
Lely A2	1.684	3.282	6.660	21.862
North Hoyle	1.739	3.535	33.547	118.600
Irene Vorrink	2.059	5.234	4.371	22.876

As all the towers are tapered, EI_η is an equivalent tower stiffness which, according to Bhattacharya (2011) may be evaluated as

$$EI_\eta = (EI)_{top} \times f_p(m) \tag{36}$$

Where, $f_p(m) = \frac{1}{3} \times \frac{2m^2(m-1)^3}{2m^2 \ln(m) - 3m^2 + 4m - 1}$ and $m = D_{bottom}/D_{top}$ is the ratio of the tower bottom diameter to its top diameter.

The Table 11 gives the different parameters required to compute the equivalent tower bending stiffness.

The different values of the non-dimensional parameters η_L , η_R and η_{LR} are given in the

following Tables 12 and 13.

The coefficients appearing in the expressions (34) and (35) rely on values of η_L , η_R and η_{LR} . Tables 14 and 15 show the values of these coefficients for the four wind turbines chosen in this paper.

The final values of the natural frequency for each wind turbine are given in Tables 16 and 17. Also shown in these tables the measured frequency in each wind farm considered here as well as natural frequencies based on the DNV codes for comparison purposes. The natural frequencies corresponding to the DNV code are based on the values of stiffnesses reported in this code, and

Table 12 η_L , η_R and η_{LR} for Walney 1 and Lely A2

Soil profiles	Interface	WALNEY 1			LELY A2		
		η_L	η_R	η_{LR}	η_L	η_R	η_{LR}
Gibson's	Rough	41212.699	2041.427	-8309.867	54426.395	8456.231	-19596.700
	Smooth	32910.910	1575.863	-6623.277	44403.943	6689.849	-15928.313
Parabolic variation	Rough	26928.490	1659.333	-5879.476	27679.088	4691.486	-10016.010
	Smooth	21811.981	1244.180	-4687.174	23031.564	3686.917	-8252.995

Table 13 η_L , η_R and η_{LR} for North Hoyle and Irene Vorrink

Soil profiles	Interface	NORTH HOYLE			IRENE VORRINK		
		η_L	η_R	η_{LR}	η_L	η_R	η_{LR}
Gibson's	Rough	423775.110	56475.467	-142524.276	88707.298	7559.107	-23632.864
	Smooth	353485.180	45827.003	-118216.180	72204.068	5964.220	-19168.133
Parabolic variation	Rough	166298.157	21106.205	-52035.515	46356.819	4371.246	-12512.839
	Smooth	142282.188	17412.842	-44366.528	38460.661	3417.778	-10273.441

Table 14 C_R and C_L for Walney 1 and Lely A2

Soil profiles	Interface	WALNEY 1		LELY A2	
		C_R	C_L	C_R	C_L
Gibson's	Rough	0.99546541	0.99972931	0.99881117	0.99977813
	Smooth	0.99318627	0.99960596	0.99829551	0.99969141
Parabolic variation	Rough	0.99558259	0.99967202	0.99844053	0.99968242
	Smooth	0.99301541	0.99951878	0.99772081	0.99956137

Table 15 C_R and C_L for North Hoyle and Irene Vorrink

Soil profiles	Interface	NORTH HOYLE		IRENE VORRINK	
		C_R	C_L	C_R	C_L
Gibson's	Rough	0.99980492	0.9999688	0.99868211	0.99986508
	Smooth	0.99973518	0.99995879	0.99810021	0.99981136
Parabolic variation	Rough	0.99965463	0.99994738	0.99832562	0.99981025
	Smooth	0.99953446	0.9999316	0.99753177	0.99973621

Table 16 Natural frequency f_η for Walney 1 and Lely A2

Soil profiles	Interface	WALNEY 1			LELY A2		
		Predicted frequency $f_\eta = C_R C_L f_{FB}$		Measured frequency	Predicted frequency $f_\eta = C_R C_L f_{FB}$		Measured frequency
		Present study	DNV		Present study	DNV	
Gibson's	Rough	0.3453	0.3342	0.35	0.7672	0.7413	0.634
	Smooth	0.3445			0.7668		
Parabolic variation	Rough	0.3453	0.3315		0.7669	0.7369	
	Smooth	0.3444			0.7662		

Table 17 Natural frequency f_η for North Hoyle and Irene Vorrink

Soil profiles	Interface	NORTH HOYLE			IRENE VORRINK		
		Predicted frequency $f_\eta = C_R C_L f_{FB}$		Measured frequency	Predicted frequency $f_\eta = C_R C_L f_{FB}$		Measured frequency
		Present study	DNV		Present study	DNV	
Gibson's	Rough	0.4479	0.4170	0.35	0.5510	0.5187	0.546-0.56
	Smooth	0.4478			0.5506		
Parabolic variation	Rough	0.4478	0.4127		0.5508	0.5143	
	Smooth	0.4477			0.5503		

which are inaccurate in our opinion as they have been established on the basis of long slender piles whose behavior differs enormously from that of short monopiles. Smoothness or roughness of the soil/monopile interface is not taken into account in these expressions.

Four important points emerge from the close examination of these two Tables 16 and 17. Firstly, the measured frequencies corresponding to the turbines belonging to both sites Lely A2 and North Hoyle are less than those corresponding to fixed base cases. This does not make sense and it is an unrealistic situation as the fixed base frequency corresponds to a tower embedded in a medium whose stiffness has an infinite value. In other words it is the maximum value that may be reached. This is may be due to the errors in the measures reported in the literature. For this reason, the comparison could not take place, and hence it useful to reconsider the frequency measurement and soil and turbine data for these two wind farm sites. Secondly, a close agreement is obtained between the measured frequencies and those obtained from this study for both turbines of Walney 1 and Irene Vorrink. Our values are better than those obtained using the DNV code. Thirdly, a very insignificant effect of the interface properties on the values of the computed natural frequency of all turbines considered here. Fourthly, the pattern of soil stiffness variation with depth has practically no effect on the computed values of natural frequency. This is noticed in all turbines for the four sites.

7. Conclusions

Wind turbines supported on monopile foundations are dynamically sensitive and are currently

designed to have a life of 25 to 30 years. Any change in soil properties will alter the dynamics of the overall system as they fundamentally derive their stiffness from the surrounding soil. Therefore the prediction of the long term performance, in depth study on dynamic soil-structure interaction is often required.

As far as the accurate determination of the monopile head stiffnesses is concerned, the finite element method is the most powerful numerical method that may be used in dealing with the aforementioned problem. Indeed, the semi-analytical finite element method has been used in this paper to address the problem. This procedure combines the finite element analysis which is based on the 2D discretization in the radial plane with the expansion of displacements and forces in Fourier series in the circumferential direction.

The problem has been analyzed for a non-homogeneous half space being characterized by a soil modulus whose evolution with depth is either linear or parabolic. For these kinds of soils, and for the two extreme interface states (rough and smooth), a comprehensive parametric study involving the variation the monopile head stiffnesses in function of (L_p/D_p) has been carried out. Finite element results were presented for two (02) Poisson's ratios $\nu_s = 0.40$ and $\nu_s = 0.499$. Analytical expressions for the impedance functions for monopiles have been established. Comparison with the existing solutions for the few available cases reveals the consistency of the proposed method.

The obtained expressions of lateral stiffness coefficient K_L , rocking stiffness K_R and cross coupling stiffness coefficient K_{LR} were incorporated in the analytical expression for the natural frequency which encompasses these three parameters. Four wind turbines have been chosen from wind farm sites available in the literature and for which the measured natural frequencies are known. The good agreement obtained between the numerical results and those of measured ones demonstrate the ability of present formulation to predict correct natural frequencies and show the inappropriateness of the design codes (DNV among others) to design short monopiles supporting offshore wind turbines.

References

- Achmus, M., Kuo, Y.-S. and Abdel-Rahman, K. (2009), "Behavior of monopile foundations under cyclic lateral load", *Comput. Geotech.*, **36**(5), 725-735.
- Adhikari, S. and Bhattacharya, S. (2011), "Vibrations of wind-turbines considering soil-structure interaction", *Wind Struct.*, **14**(2), 85-112.
- Adhikari, S. and Bhattacharya, S. (2012), "Dynamic analysis of wind turbine towers on flexible foundations", *Shock Vib.*, **19**(1), 37-56.
- Al Hamaydeh, M. and Hussain, S. (2011), "Optimized frequency-based foundation design for wind turbine towers utilizing soil-structure interaction", *J. Franklin Inst.*, **348**(7), 1470-1487.
- Amar Bouzid, Dj. (1997), "Analyse semi-analytique par éléments finis des pieux isolés sollicités horizontalement dans un milieu à comportement non-linéaire", Thèse de Magister, Ecole Nationale Polytechnique, Alger, Algérie.
- Amar Bouzid, Dj., Tiliouine, B. and Vermeer, P.A. (2004), "Exact formulation of interface stiffness matrix for axisymmetric bodies under non-axisymmetric loading", *Comput. Geotech.*, **31**(2), 75-87.
- American petroleum Institute (API) and International Organization for Standardization (ISO) (2011), ANSI/API Specification RP 2GEO, *Geotechnical Considerations and Foundation Design for Offshore Structures*. Washington, DC.
- Andersen, L.V., Vahdatirad, M.J., Sichani, M.T. and Sorensen, J.D. (2012), "Natural frequencies of wind turbines on monopile foundations in clayey soils-A probabilistic approach", *Comput. Geotech.*, **43**, 1-11.

- Bhattacharya, S. (2011), *SDOWT: Simplified Dynamics of Wind Turbines*, User's Manual, Bristol Laboratory for Advanced Dynamics Engineering, Bristol, UK.
- Bhattacharya, S. (2014), "Challenges in design of foundations for offshore wind turbines", *Eng. Technol. Reference*, **1**(1), 1-9.
- Bhattacharya, S., Cox, J.A., Lombardi, D. and Wood, D.M. (2013), "Dynamics of offshore wind turbines supported on two foundations", *Proc. Inst. Civ. Eng.: Geotech. Eng.*, **166**(GE2), 159-169.
- Bisoi, S. and Haldar, S. (2015), "Design of monopile supported offshore wind turbine in clay considering dynamic soil-structure-interaction", *Soil Dyn. Earthq. Eng.*, **73**, 103-117.
- Booker, J.R., Baalam, N.P. and Davis, E.H. (1985), "The behavior of an elastic non-homogenous half-space", *Int. J. Numer. Anal. Meth. Geomech.*, 353-367.
- Burland, J.B., Sills, G.C. and Gibson, R.E. (1973), "A field and theoretical study of the interface of non-homogeneity on settlement", *Proceedings of the 8th International Conference on Soil Mechanics*, Moscow.
- Cole, K.W. and Burland, J.B. (1972), "Observations of retaining wall movements associated with a large excavation", *Proceedings of 5th European Conference on Soil Mechanics*, Madrid.
- Cook, R.D., Malkus, D.S., Plesha, M.E. and Witt, R.J. (2002), *Concepts and Applications of Finite Element Analysis*, Joh Wiley and Sons inc., New York, USA.
- Cuéllar, P., Georgi, S., Baessler, M. and Rücker, W. (2012), "On the quasi-static granular convective flow and sand densification around pile foundations under cyclic lateral loading", *Granular Matter*, **14**(1), 11-25.
- Damgaard, M., Bayat, M., Andersen, L.V. and Ibsen, L.B. (2014), "Assessment of the dynamic behavior of saturated soil subjected to cyclic loading from offshore monopile wind turbine foundations", *Comput. Geotech.*, **61**, 116-126.
- Damgaard, M., Bayat, M., Andersen, L.V. and Ibsen, L.B. (2015), "Dynamic response sensitivity of an offshore wind turbine for varying subsoil conditions", *Ocean Eng.*, **101**, 227-234.
- Davies, T.G. and Budhu, M. (1986), "Non linear analysis of laterally loaded piles in heavily overconsolidated clays", *Géotechnique*, **36**(4), 527-538.
- Det Norske Veritas (2004), *DNV-OS-J101 Offshore standard: Design of offshore wind turbine structures*, Hellrup, Danmark: DNV.
- Durocher, L.A., Gasper, A. and Rhoades, G. (1978), "A numerical comparison of axisymmetric finite elements", *Int. J. Numer. Meth. Eng.*, **12**(9), 1415-1427.
- Gazetas, G. (1991), *Foundation vibrations*, In *Foundation Engineering Handbook*, 2nd Edition, Ed., Fang, H-Y., Van Nostrand Reinhold, New York, 553-593.
- GL (2005), Rules and guidelines - Industrial services, Germanischer Lloyd.
- Griffiths, D.V. and Lane, P.A. (1990), "Finite element analysis of the shear vane test", *Comput. Struct.*, **37**(6), 1105-1116.
- Higgins, W., Vasquez, C., Basu, D. and Griffiths, D.V. (2013), "Elastic solutions for laterally loaded piles", *J. Geotech. Geoenviron. Eng.*, **139**(7), 1096-1103.
- Hooper, J.A. (1973), "Observations on the behavior of a piled raft foundation on London clay", *Proceeding of the Institution Civil Engineering*.
- Laszlo, A., Bhattacharya, S., Hogan, S.J. and Macdonald, J. (2014), "Dynamic soil-structure interaction issues of offshore wind turbines", *Proceedings of the 9th International Conference on Structural Dynamics*, Porto, Portugal.
- Leblanc, C. (2009), "Design of offshore wind turbine support structures-selected topics in the field of geotechnical engineering", Aalborg University, Denmark.
- Lombardi, D., Bhattacharya, S. and Wood, D.M. (2013), "Dynamic soil-structure interaction of monopile supported wind turbines in cohesive soil", *Soil Dyn. Earthq. Eng.*, **49**, 165-180.
- Luqing, Y., Bhattacharya, S., Lingling, L. and Zhen, G. (2014), "Dynamic characteristics of offshore wind turbines on different types of foundations", *Electron. J. Geotech. Eng.*, **19**, 2917-2936.
- Matlock, H. (1970), "Correlations for design of laterally loaded piles in soft clay", *Proceedings of the Offshore Technology Conference*, Houston, Texas.

- Murchison, J.M. and O'Neill, M.W. (1984), "Evaluation of p-y relationships in cohesionless soils", *Analysis and Design of Pile Foundations, Proceedings of a Symposium in conjunction with the ASCE National Convention*, pp. 174-191.
- Myers, A.T., Arwade, S.R., Valamanesh, V., Hallowell, S. and Carswell, W. (2015), "Strength, stiffness, resonance and the design of offshore wind turbine monopoles", *Eng. Struct.*, **100**, 332-341.
- Potts, D.M. and Zdrackovic, L. (1999), *Finite Element Analysis in Geotechnical Engineering: Theory*. Thomas Telford Publishing, Heron Quay, London, UK.
- Poulos, H.G. and Hull, S.T. (1989), "Analytical geomechanics in foundation engineering- A study of laterally loaded piles", Research Report No. R667. School of Civil and Mining Engineering, Sydney University.
- Poulos, H.G. and Davis, E.H. (1980), *Pile foundation analysis and design*, Wiley, New York, USA.
- Prendergast, L.J., Gavin, K. and Doherty, P. (2015), "An investigation into the effect of scour on the natural frequency of an Offshore Wind Turbine", *Ocean Eng.*, **101**, 1-11
- Randolph, M.F. (1981), "The response of flexible piles to lateral loading", *Géotechnique*, **31**(2), 247-259.
- Reese, L., Cox, W.R. and Koop, F.D. (1974), "Analysis of laterally loaded piles in sand", OTC 2079, *Proceedings of the Offshore Technology Conference*, Houston, USA.
- Shirzadeh, R., Devriendt, C., Bidakhvidi, M.A. and Guillaume, P. (2013), "Experimental and computational damping estimation of an offshore wind turbine on a monopile foundation", *J. Wind Eng. Indust. Aerodyn.*, **120**, 96-106.
- Tempel, D.P. and Molenaar, D.P. (2002), "Wind turbine structural dynamics- a review of the principles for modern power generation, onshore and offshore", *Wind Eng.*, **26**(4), 211-220.
- Vught, J.H. (2000), "Considerations on the dynamics of support structures for an offshore wind energy converters", Ph.D thesis, Delft University of Technology, The Netherlands.
- Wilson, E.L. (1965), "Structural analysis of axisymmetric solids", *J. Am. Inst. Aeronaut Astronaut*, **3**(12), 2269-2274.
- Winnicki, L.A. and Zienkiewicz, O.C. (1979), "Plastic (or visco-plastic) behavior of axisymmetric bodies subjected to non-axisymmetric loading, semi-analytical finite element solution", *Int. J. Numer. Meth. Eng.*, **14**(9), 1399-1412.
- Yi, Jin-Hak, Sun-Bin, Kim, Gil-Lim, Yoon and Lars Vabbersgaard, Andersen (2015), "Natural frequency of bottom-fixed offshore wind turbines considering pile-soil-interaction with material uncertainties and scouring depth", *Wind Struct.*, **21**(6), 625-639.
- Yu, Lu-Qing, Li-Zhong, Wang, Zhen, Guo, S., Bhattacharya, G., Nikitas, Ling-Ling, Li and Yue-Long, Xing (2015), "Long-term dynamic behavior of monopile supported offshore wind turbines in sand", *Theo. Appl. Mech. Lett.*, **5**(2), 80-84.
- Zienkiewicz, O.C. and Taylor, R.L. (2000), *The Finite Element Method*, Butterworth-Heinemann, London, UK.